Course objectives

1. Gain experience with the principal computational tools used for preliminary aerodynamic (subsonic) design of airfoils, wings, whole vehicles
    - Airfoils: Panel+BL method: viscous/inviscid interaction (VII) - exemplified by XFOIL
    - Wings/whole vehicles: Vortex lattice methods (VL) - exemplified by AVL;

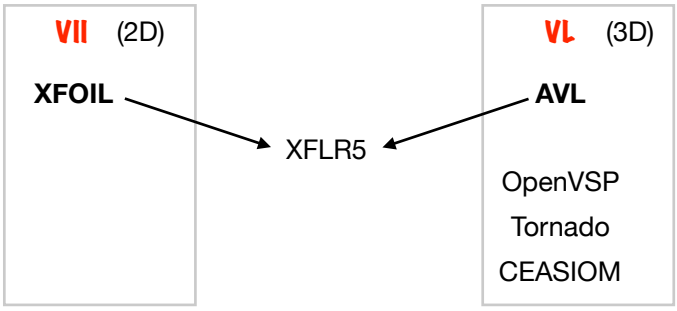

2. Gain an appreciation of transonic aerodynamics of airfoils and (swept) wings, including flow remediation methods;
3. Be able to estimate maximum lift coefficients for wings/high angles of attack;
4. Be able to derive aerodynamic and inertial loads on wings, carry out preliminary structural design;
5. Understand the bases of optimal aerodynamic design of airfoils and wings.

Outline of Topical Organisation

1. Relevant fluid mechanics
    - inviscid/viscous/incompressible/compressible/singularity lumping
2. Airfoil aerodynamics
    - Characterisation of airfoils
    - Inviscid analysis
    - Boundary layer modelling
    - Viscous–inviscid interaction
    - Case studies
3. Wing aerodynamics
    - Inviscid methods
    - Trefftz plane drag analysis
    - Planform, twist, airfoil choice
4. Transonic aerodynamics
    - Airfoils
    - Wing sweep
    - Area rule
5. Wing structure and design
    - Wing as a beam/load relief, Structure
6. High-lift aerodynamics, aerodynamic remediation, direct/inverse design methods

Revision

Knowledge assumed from earlier courses

1. Euler and Navier–Stokes equations, Bernoulli's equation
2. Control volume analysis
3. Similitude and dimensional analysis, similarity-based flow solutions
4. Analytical thin airfoil theory
5. Prandtl's lifting line analysis
6. Potential flows and construction of flow fields by superposition
7. Laminar and turbulent boundary layers, transition
8. Boundary layer equation and integral treatment of equation
9. Properties of normal and oblique shock waves
10. Linearized compressible flow, critical Mach number
11. Key aspects of aircraft performance including use of drag polar
12. Introductory material on airfoils and finite wings

New in this course

Linear inviscid aerodynamics tools

1. Discrete methods for thin airfoil analysis
2. Panel methods for inviscid finite-thickness airfoil analysis (XFOIL)
3. Vortex lattice methods for inviscid finite-wing and complete-vehicle aerodynamics (AVL)

Viscous boundary layers and VII tools

1. Numerical treatment of wall-normal integrated boundary-layer equations
2. Prediction of BL transition to turbulence using the e^N method
3. Viscous-Inviscid Interaction for airfoil aerodynamic analysis (XFOIL)

Wings with sweep

1. Aerodynamics of swept wings and wing-body assemblies – subsonic, transonic, supersonic
2. High-α subsonic aerodynamics for highly-swept surfaces
3. Aerodynamic crutches – flow remediation tools for swept wings

Other

1. Airfoil and wing design for transonic flight
2. Wing design parameters
3. Wing structural loading and design
4. Introduction to codified design tools (ESDU)
5. High-lift aerodynamic estimation for airfoils using correlation-based methods
6. Inverse methods and design optimisation

References and reading

Anderson JD, *Fundamentals of Aerodynamics*, 5e, McGraw Hill 2011.

Bertin JJ & Cummings RM, *Aerodynamics for Engineers*, 5e, Prentice-Hall 2009.

Drela M, *Flight Vehicle Aerodynamics*, MIT Press 2014 (available as PDF from Monash Library).

Engineering Sciences Data Unit (ESDU), various items.

Katz J & Plotkin A, *Low-Speed Aerodynamics*, 2e, Cambridge 2001 (available as PDF from Monash Library).

Howe D, *Aircraft Loading and Structural Layout*, AIAA 2004.

Kuethe AM & Chow C-Y, *Foundations of Aerodynamics*, 4e, Wiley 1986.

McCormick BW, *Aerodynamics, Aeronautics, and Flight Mechanics*, 2e, Wiley 1995.

McLean D, *Understanding Aerodynamics*, Wiley 2013 (available as PDF from Monash Library).

Obert E, *Aerodynamic Design of Transport Aircraft*, IOS Press 2009.

Schlichting HT & Truckenbrodt EA, *Aerodynamics of the Aeroplane*, 2e, McGraw-Hill 1979.

Torenbeek E, *Synthesis of Subsonic Airplane Design,* Martinus Nijhoff Pubs 1986.

Torenbeek E, *Advanced Aircraft Design*, Wiley 2013 (available as PDF from Monash library).

Torenbeek E & Wittenberg H, *Flight Physics*, Springer 2009 (available as PDF from Monash library).

- Airfoil Coordinates Database (UIUC): http://www.uiuc.edu/ph/www/m-selig/ads/coord_database.html.

- A/C design by I. Kroo (Stanford): http://aero.stanford.edu/aa241/AircraftDesign.html
- A/C design by W.H. Mason (Virginia Tech): http://www.aoe.vt.edu/Mason/ACinfoTOC.html

Wing design

The wing is the single most important aircraft component.

Typical wing design objectives:

1. Maximize aerodynamic efficiency, i.e. minimize drag for design lift coefficient
2. Maximize $C_{L\max}$ (landing/manouevring)
3. Good flight handling qualities (stall/spin)
4. Safety (min. rate of climb, 1 engine out)
5. Maximize thickness/internal volume (fuel)
6. Maximize strength (manouevring)
7. Minimize structural weight (wing loading)
8. Maximize stiffness (divergence/flutter)
9. Minimize manufacturing costs
10. Ground handling/stowage

These requirements may conflict and there may be a number of design points to consider (e.g. sub/supersonic flight segments).

The main tasks of wing aerodynamic design are to select wing airfoils and planform to best achieve the design goals.

No unique answers!

Two very different wing designs for nominally the same requirement can give similar *L/D* and overall performance.

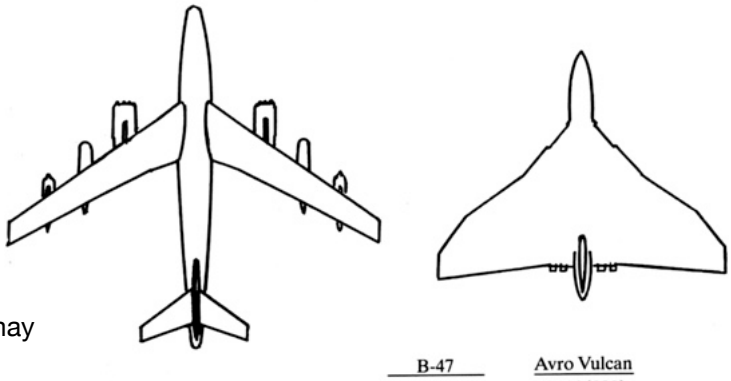

	B-47	Avro Vulcan
S reference	1430 {132}	3446 {320}
S wetted	11300 {1050}	9600 {892}
Span	116 {35}	90 {27}
Swet/ Sref	7.9 {7.9}	2.8 {2.8}
Aspect ratio	9.4 {9.4}	3.0 {3.0}
Wetted aspect ratio	1.2 {1.2}	1.1 {1.1}
L/D max	17.2 {17.2}	17.0 {17.0}

Raymer

Aircraft efficiency and range

Breguet range equation assuming constant C_L cruise

$$R = V\frac{L}{D}\frac{1}{\mathrm{g}c_t}\ln\frac{W_0}{W_1} \qquad \text{(for jets)}$$

More generally, since $\eta_o P_C = TV$ where P_C is power derived from conversion of chemical energy, and η_o is overall energy conversion efficiency, and $P_C = H\dot{m}_f$ in which H is the heating value of fuel ($H \simeq 42$ MJ/kg for most hydrocarbon fuels), $\dot{m}_f$ is fuel mass flow rate;

$$\eta_o H\dot{m}_f = \frac{\dot{m}_f}{c_t}V \quad \text{so that} \quad \frac{V}{\mathrm{g}c_t} = \eta_o\frac{H}{\mathrm{g}}$$

This form of range equation works for any type of fuel-burning aircraft, prop or jet, because it is based on power output rather than thrust.

and $R = \eta_o\frac{H}{\mathrm{g}}\frac{L}{D}\ln\frac{W_0}{W_1}$

structural efficiency

propulsion system efficiency

fuel type

aerodynamic efficiency

Similar equations can be developed for endurance, or non-fuel-burning propulsion (e.g. batteries).

This initially seems like a straightforward division of optimisation targets but in reality, aerodynamics and structures are coupled through the weight ratio W_0/W_1.

Aircraft efficiency and range

$$R = \eta_o\frac{H}{\mathrm{g}}\frac{L}{D}\ln\frac{W_0}{W_1}$$

Suppose $W_1 = W_e$ = aircraft empty weight with all fuel consumed, and $W_0 = W_e + W_f$ where W_f = fuel weight.

$$R = \eta_o\frac{H}{\mathrm{g}}\frac{L}{D}\ln\frac{W_e + W_f}{W_e} = \eta_o\frac{H}{\mathrm{g}}\frac{L}{D}\ln\left(1 + \frac{W_f}{W_e}\right)$$

$\frac{W_f}{W_e}$	$\ln\left(1+\frac{W_f}{W_e}\right)$
1	0.693
0.5	0.406
0.25	0.233

For large transport aircraft, the wing typically contributes of order 40% of W_e and houses all the fuel, W_f.

Recall: $L/D_{\max} = \frac{1}{2}\sqrt{\frac{\pi Ae}{C_{D,0}}}$

An "obvious" way to increase *L/D* is to increase wing aspect ratio *A,* but for the same wing area and loading, that will also increase wing weight to meet a given load factor *n*, owing to increase in wing-root bending moment and consequent increase in required strength. Hence increasing *A* will increase W_e (and directly decreases the amount of possible stored fuel, W_f, since wing volume is inversely proportional to A for given S).

This means that in reality, overall wing design optimisation (e.g. to reduce overall aircraft weight and fuel use) requires coupled consideration of structure and aerodynamics, typically iteratively. However, in this subject the two aspects are treated as decoupled.

Wing typology

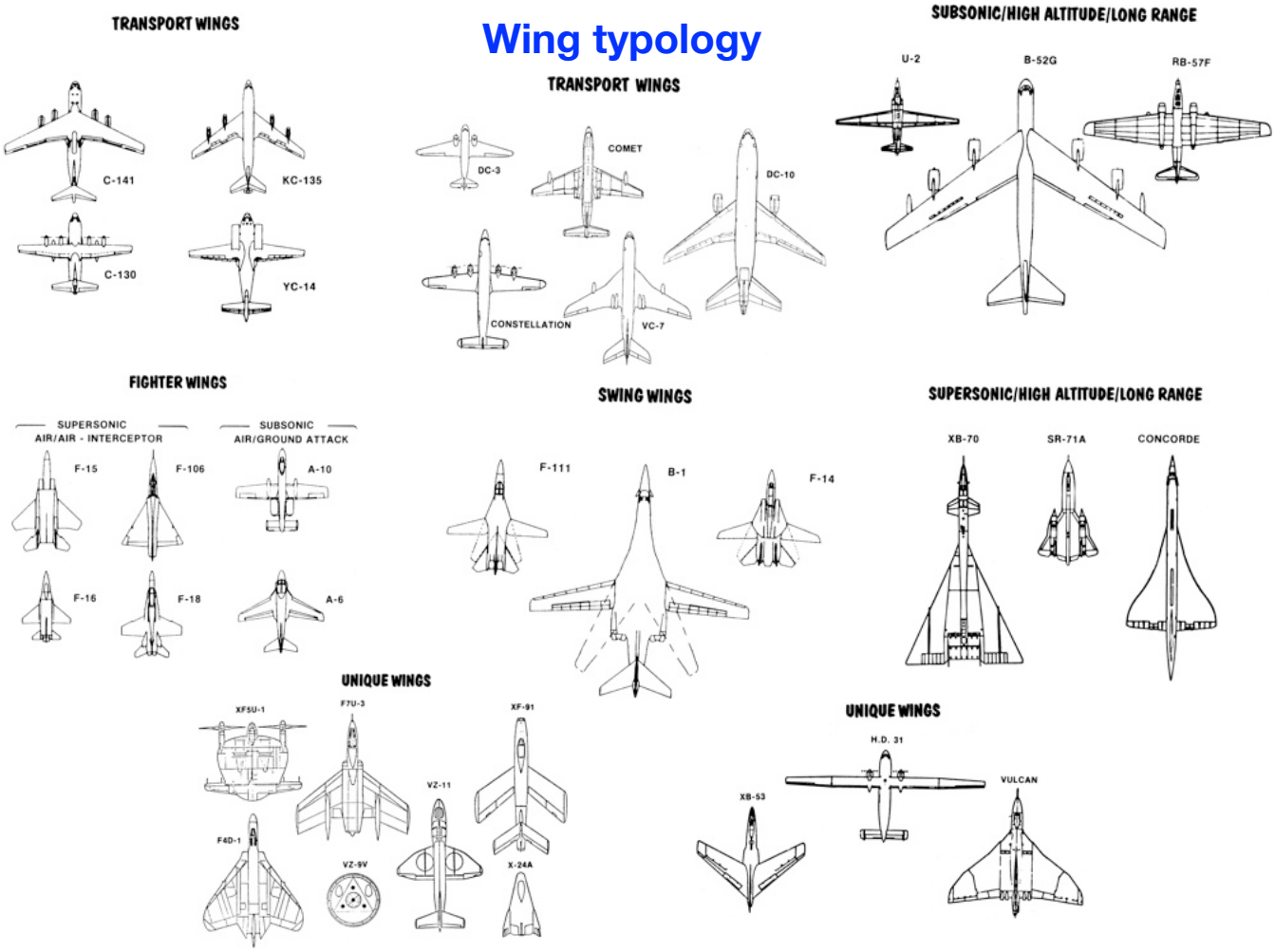

Overview perspective on wing aerodynamics

1. Most aircraft operate at large Reynolds numbers, and moderate-or-low Mach numbers. Our focus here is on subsonic/transonic wings (i.e. the vast majority).
2. For efficiency (good L/D), most wings are of moderate-to-high aspect ratio ($A = b^2/S > 4$, say).
3. Again for efficiency, aircraft geometries have evolved to be highly streamlined, i.e. to produce only minor flow separations. (Persistent flow separation is of major concern to the aerodynamicist.)
4. Flows around high-aspect ratio wings are dominated by 2D; 3D effects are small corrections to 2D though their spanwise-integrated effects (e.g. induced drag) are possibly large.
5. Conversely, boundary-layer flows are predominantly dealt with using 1D methods and have negligible effect on 3D flows (since their length scale/thickness is tiny compared to other aircraft lengths), and only minor effect on 2D airfoil flows. BL turbulence is dealt with using correlations.
6. Hence there is a natural subdivision in design/analysis methods for 2D (airfoil) and 3D (whole wing/vehicle) flows.
7. On the assumption that flows remain attached, inviscid analysis methods are enough for most 3D whole-vehicle design tasks. A combination of coupled inviscid and viscous (BL) methods has been evolved for 2D airfoil flows. Full 3D RANS solvers of the type offered by Ansys are little used until final design iterations, with experimental spot checks (this is a cost-based progression).
8. About the only time highly separated flows can be tolerated is during flight phases which do not persist for long (so overall impact on energy use is small). This amounts to take-off and landing segments or brief manoeuvres. We will consider some specialised tools for such flows, particular to highly swept wings at large angle of attack.
9. A number of flow remediations ("aerodynamic crutches") have been evolved to help control/ suppress some types of flow separations. We will also review these.
10. Another review area will deal with transonic/shock effects on 2D/3D wing flows.

Revision fluid mechanics

Reading: Anderson Chs 2, 3, 11.

Revision

The production of lift — circulation

The fundamental results of classical aerodynamics (for incompressible flows) are

1. Kutta–Joukowsky theorem relates lift per unit length to circulation around a loop bounding vorticity in the flow:

$$l = \rho V_\infty \Gamma$$

$$\Gamma = \oint_C \boldsymbol{u} \cdot \mathrm{d}\boldsymbol{r} = \int_S \boldsymbol{n} \cdot \boldsymbol{\omega}\, \mathrm{d}A$$

Where C is a closed curve bounding surface S.

2. Kelvin's theorem (a.k.a. Helmholtz's theorems) for inviscid barotropic fluid

i. Fluid elements initially free of vorticity remain free of vorticity.
ii. Fluid elements lying on a vortex line at some instant continue to lie on that vortex line. More simply, vortex lines move with the fluid.
iii. The strength of a vortex tube does not vary with time. $\dfrac{\mathrm{D}\Gamma}{\mathrm{D}t} = \dfrac{\mathrm{D}}{\mathrm{D}t} \oint_C \boldsymbol{u} \cdot \mathrm{d}\boldsymbol{r} = 0$

Corollary: vortex lines and tubes must appear as a closed loop or extend to infinity or start/end at solid boundaries. A vortex line has constant strength along its length.

3. Biot–Savart law: a segment of a general curvilinear vortex filament of strength Γ `induces' velocity at a remote location:

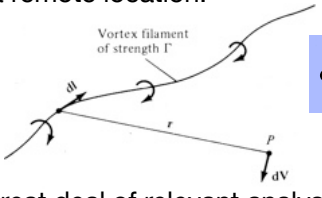

$$\mathrm{d}\boldsymbol{V} = \frac{\Gamma}{4\pi} \frac{\mathrm{d}\boldsymbol{l} \times \boldsymbol{r}}{|\boldsymbol{r}^2|}$$

The effect of the whole filament is obtained by integration:

$$\boldsymbol{V} = \int_{-\infty}^{\infty} \frac{\Gamma}{4\pi} \frac{\mathrm{d}\boldsymbol{l} \times \boldsymbol{r}}{|\boldsymbol{r}^2|}$$

A great deal of relevant analysis and design can be done based on these theorems, and assuming that viscous effects (and vorticity, friction) is confined to small (singular) regions. This works because Reynolds numbers are typically very high, making these assumptions quite reasonable.

In turn, we can often invoke principles of linearity and superposition in the analysis.

Revision

Potential flows (recap)

An irrotational incompressible flow can be described in terms of two (alternative) scalar functions, the velocity potential and the stream function. Either of these satisfies Laplace's equation for such flows.

1. The velocity potential

Flow is irrotational (vorticity=0) $\boldsymbol{\omega} = \boldsymbol{\nabla} \times \boldsymbol{u} = 0$ Vector identity $\boldsymbol{\omega} = \boldsymbol{\nabla} \times \nabla\phi = 0$

Propose $\boldsymbol{u} = \nabla\phi$ $u = \dfrac{\partial\phi}{\partial x}; \quad v = \dfrac{\partial\phi}{\partial y}; \quad w = \dfrac{\partial\phi}{\partial z}$ automatically irrotational

Flow also incompressible $\boldsymbol{\nabla} \cdot \boldsymbol{u} = 0$ Satisfies Laplace's equation $\boldsymbol{\nabla} \cdot \boldsymbol{u} = \boldsymbol{\nabla} \cdot \nabla\phi = \nabla^2\phi = 0$

Typical (solid-wall) boundary condition $\dfrac{\partial\phi}{\partial n} = \nabla\phi \cdot \boldsymbol{n} = 0$ where ***n*** is a unit vector, normal to the wall

2. The stream function (2D)

Flow is incompressible $\boldsymbol{\nabla} \cdot \boldsymbol{u} = \dfrac{\partial u}{\partial x} + \dfrac{\partial w}{\partial z} = 0$

Propose $u = \dfrac{\partial\psi}{\partial z}; \quad w = -\dfrac{\partial\psi}{\partial x}$ $\boldsymbol{\nabla} \cdot \boldsymbol{u} = \dfrac{\partial^2\psi}{\partial x \partial z} - \dfrac{\partial^2\psi}{\partial z \partial x} = 0$ automatically incompressible

If flow is also irrotational $\boldsymbol{\omega}_y = \dfrac{\partial u}{\partial z} - \dfrac{\partial w}{\partial x} = \dfrac{\partial^2\psi}{\partial z^2} + \dfrac{\partial^2\psi}{\partial x^2} = 0$ or $\nabla^2\psi = 0$ Satisfies Laplace's equation

Typical (solid-wall) boundary condition $\psi = \text{const}$: the wall is a streamline of the flow, as is any line of constant ψ

Remarks

1. Lines of constant potential (normal to $\nabla\phi = \boldsymbol{u}$) are by definition also locally normal to streamlines.
2. Irrotational incompressible flows satisfy linear operator $\nabla^2( ) = 0$, so can be linearly superimposed.
3. The use of a scalar streamfunction is confined to 2D flows, velocity potential is more general.

Revision

The elementary potential flows

Flow	Picture	Velocity	Velocity potential	Stream function
Uniform flow, *x* direction	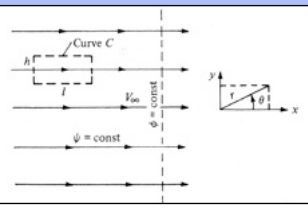	$u = V_\infty$	$V_\infty x$	$V_\infty y$
Line source/ sink	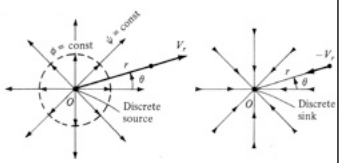	$u_r = \pm\dfrac{\Lambda}{2\pi r}$	$\pm\dfrac{\Lambda \ln r}{2\pi}$	$\pm\dfrac{\Lambda\theta}{2\pi}$
Line doublet	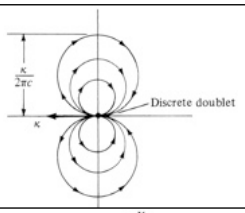	$u_r = \dfrac{M}{2\pi}\dfrac{\cos\theta}{r^2}$ $u_\theta = -\dfrac{M}{2\pi}\dfrac{\sin\theta}{r^2}$	$\dfrac{M}{2\pi r}\cos\theta$	$-\dfrac{M}{2\pi r}\sin\theta$
Line vortex	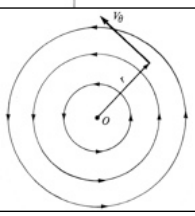	$u_\theta = -\dfrac{\Gamma}{2\pi r}$	$-\dfrac{\Gamma}{2\pi}\theta$	$\dfrac{\Gamma \ln r}{2\pi}$

Revision

The Kutta condition, circulation, and lift

Frictionless (potential) 2D flow past a plate: a variety of valid solutions can be obtained analytically:

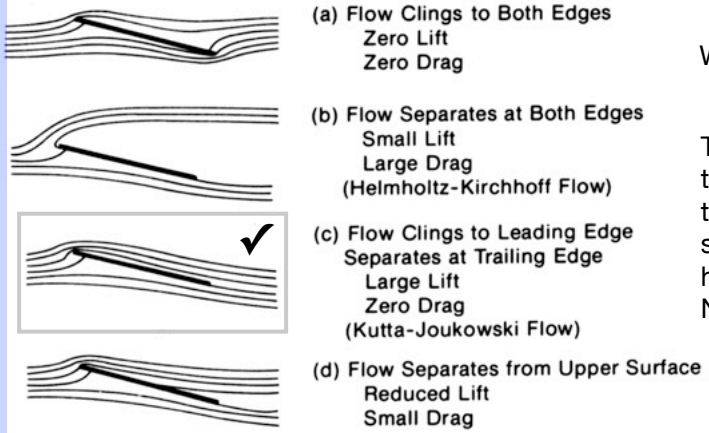

Which one is correct?

The case that best matches observed reality has the flow leaving the TE tangentially. This is called the Kutta condition and frictionless flows that satisfy it give a very good approximation to real high-*Re* attached flows, pressure distributions. Note that the ideal flow has no drag, however.

Potential flow solutions can be linearly combined to form new valid solutions: a combination of the zero-lift flow and a pure circulatory flow of correct magnitude gives a flow satisfying the Kutta condition.

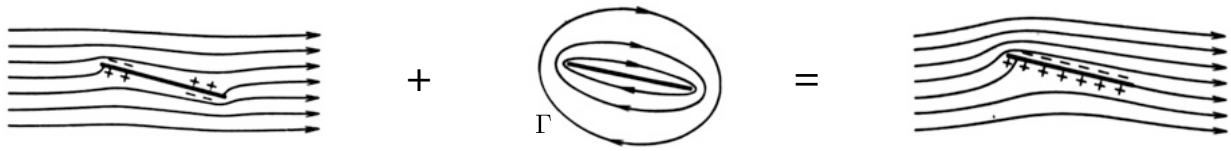

All the lift in the flow can be attributed to the circulation: an isolated vortex in a cross flow experiences lift.

Idealising a wing by a 'lifting line' vortex bound to the wing, or a sum of line vortices, allows a comparatively simple but adequate mathematical model of a finite wing and the surrounding flow to be made. These models give surprisingly accurate predictions of lift and lift-induced, as opposed to friction-related, drag.

Revision

Establishment of the Kutta condition

Images from Prandtl & Tietjens

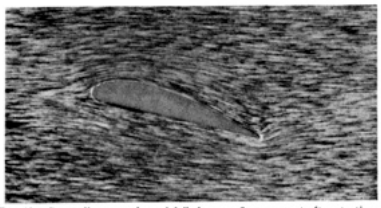

Fig. 48.—Streamlines round an airfoil the very first moment after starting.

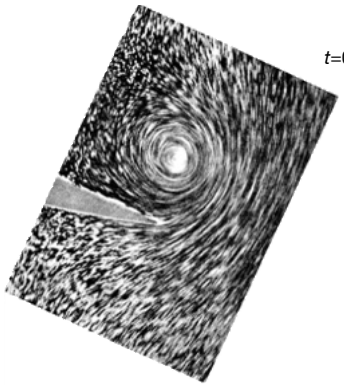

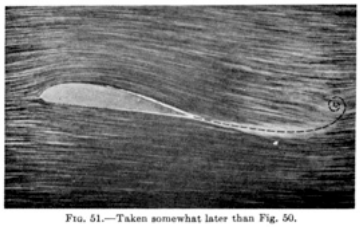

Fig. 51.—Taken somewhat later than Fig. 50.

Viscous effects force a flow separation at the TE for any real flow that does not satisfy the Kutta condition. Auto-correction of this separation provides viscous regulation of the airfoil's circulation.

Detail of TE starting flow

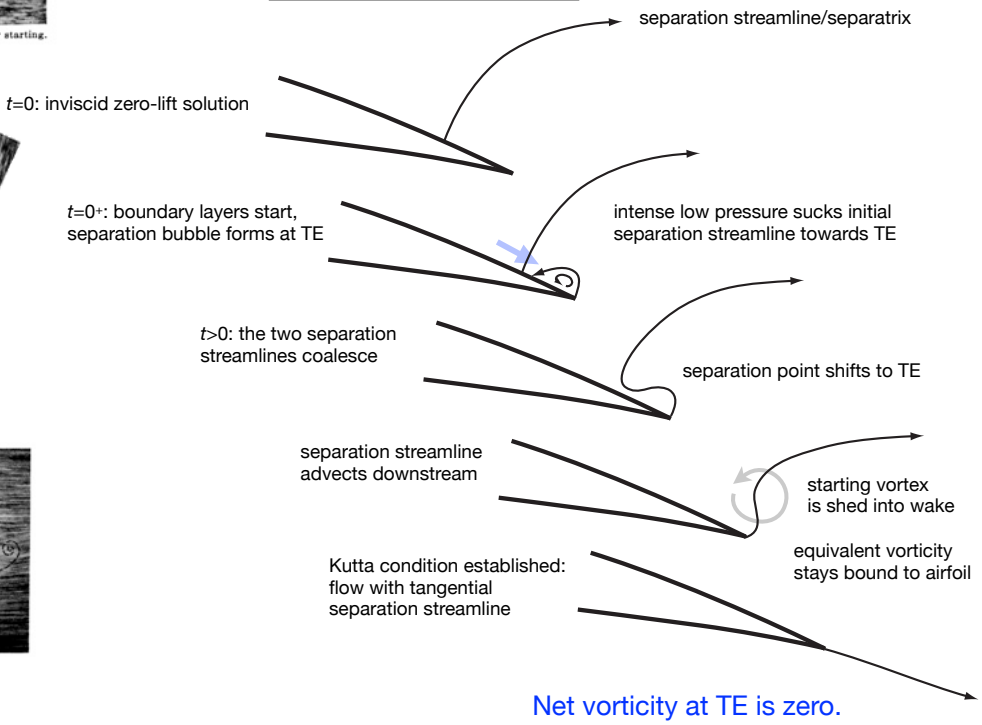

Net vorticity at TE is zero.

Revision

Drag nomenclature and mechanisms

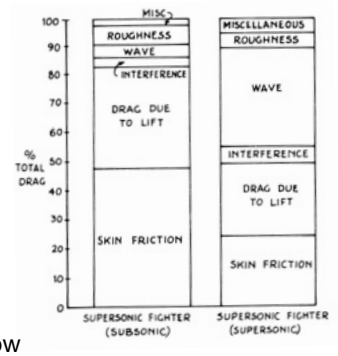

1. Total drag
   - total retarding force parallel to direction of motion
   - **total drag = skin-friction drag + pressure drag**
2. Skin-friction drag
   - drag force caused directly by skin friction/viscous traction integrated over body
3. Pressure drag
   - drag force caused by surface pressures/normal traction integrated over body
   - **pressure drag = induced drag + wave drag + form drag**
4. Induced drag
   - induced by lift/downwash, and the change in angle of attack this produces
   - does not depend directly on viscosity and can be estimated assuming inviscid flow
5. Wave drag
   - associated with pressures produced by shock waves in high-speed flight
6. Form drag (or boundary layer pressure drag)
   - the presence of boundary layers changes the external flow and hence pressures
   - this drag is caused by viscosity but is felt though its effect on pressure distribution
7. Profile drag
   - total airfoil drag attributable to viscous effects (hence is *Re* dependent)
   - **profile drag = skin friction drag + form drag**
8. Interference drag
   - drag attributable to one component (e.g. fuselage) changing flow around another (e.g. wing)
9. Trim drag
   - attributable to deflection of control surfaces - mostly this is extra induced drag
10. Parasitic drag
    - summary of all non-essential (non-lift) drag

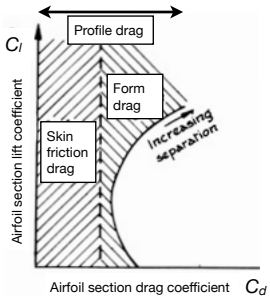

Note that the `profile drag' is associated with the wing section profile, i.e. is effectively 2D.

Revision

Typical contributions to drag for subsonic transport

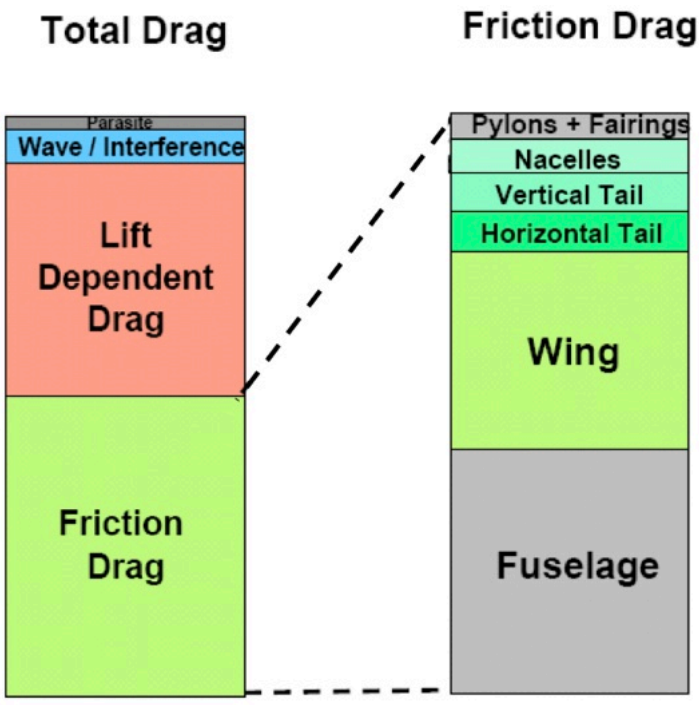

G. Schrauf, AIAA 2008

Revision

Compressibility effects — 1

1. The general progression of airfoil shock structure with Mach number:

Local supersonic flow and a compression shock arise at a 'critical' freestream M_∞<1.

For transonic flows, $M_\infty \approx 1$, the shock can produce flow separation and greatly increased drag.

Supersonic region grows to include entire upper and lower surfaces. Compression shock moves to TE.

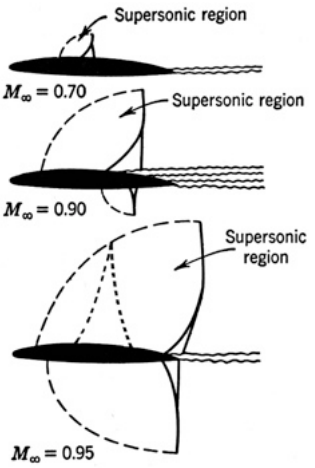

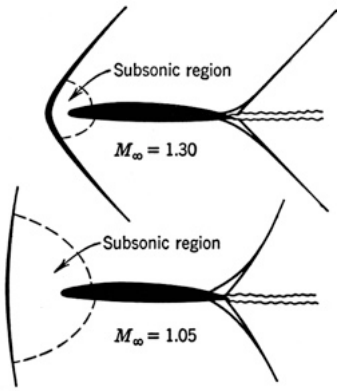

Generally, much less separation for supersonic flows but wave drag becomes dominant.

Bow shock appears at M_∞=1.

2. For isentropic (shock-free) flow, local and stagnation conditions are related through

$$\frac{\rho_0}{\rho} = \left(1 + \frac{\gamma - 1}{2} M^2\right)^{1/(\gamma-1)} \qquad \frac{p_0}{p} = \left(1 + \frac{\gamma - 1}{2} M^2\right)^{\gamma/(\gamma-1)}$$

3. Changes in density are negligible for sufficiently small M:

$$\frac{\rho_0 - \rho}{\rho} = \left(\frac{\gamma - 1}{2} M^2\right)^{1/(\gamma-1)} \leq 0.05 \implies M \leq 0.3$$

Revision

Compressibility effects — 2

4. Using $a_\infty^2 = \gamma p_\infty / \rho_\infty$ we can restate the pressure coefficient C_p, dimensionless local pressure variation:

$$C_p = \frac{p - p_\infty}{\frac{1}{2}\rho V_\infty^2} = \frac{2}{\gamma {M_\infty}^2}\left(\frac{p}{p_\infty} - 1\right)$$

5. The critical C_p for which the local Mach number M = 1, given freestream value M_∞ and assuming isentropic flow is

$$C_{p,cr} = \frac{2}{\gamma {M_\infty}^2}\left\{\left(\frac{1 + [(\gamma-1)/2]{M_\infty}^2}{1 + (\gamma-1)/2}\right)^{\gamma/(\gamma-1)} - 1\right\}$$

6. For linearized irrotational compressible flow (potential flow, small perturbations, not too close to M_∞ = 1) we have the Prandtl-Glauert correction

($C_{p,0}$ is C_p at M = 0.)

$$C_p \approx \frac{C_{p,0}}{\sqrt{1 - {M_\infty}^2}} \quad \text{and} \quad C_l \approx \frac{C_{l,0}}{\sqrt{1 - M_\infty^2}}$$

or the more accurate Karman-Tsien correction $C_p \approx \dfrac{C_{p,0}}{\sqrt{1 - {M_\infty}^2} + [{M_\infty}^2/(1 + \sqrt{1 - {M_\infty}^2})]C_{p,0}/2}$

7. Hence for any incompressible C_p (typically, the lowest value) we can estimate the critical freestream Mach number for the onset of local shock waves.

8. If we know (or compute) the airfoil C_p distribution for M = 0 at a given C_l, we can estimate the critical freestream Mach number M_c.

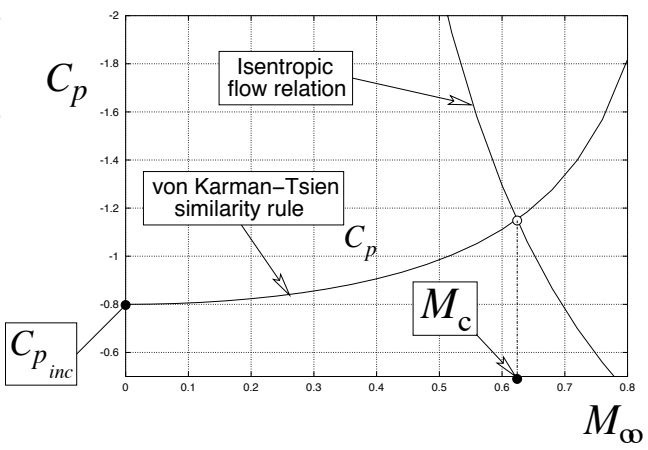

Flow-field modelling for computational methods used in wing aero analysis

Reading: Drela Chs 1 & 2.

Fluxes, forces, boundary conditions on surfaces

Fluxes

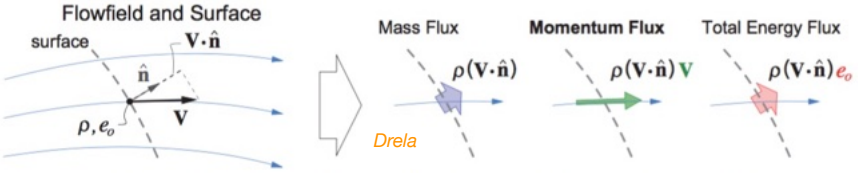

Figure 1.3: Flow-field quantities $\rho, \mathbf{V}, e_o$ together with a surface's normal vector $\hat{\mathbf{n}}$ define mass, momentum, and total internal energy fluxes across each surface point. These are associated with bulk fluid motion.

Forces

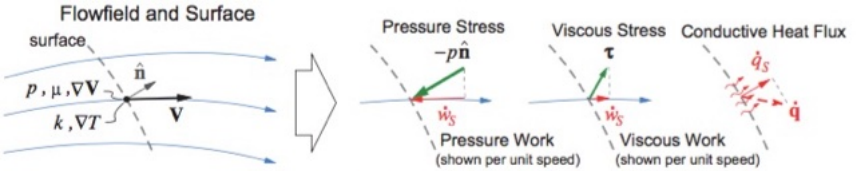

Figure 1.4: Flow-field quantities $p, \mu, \nabla\mathbf{V}$ together with a surface normal vector $\hat{\mathbf{n}}$ define pressure and viscous stress forces acting on each surface point, with corresponding work contributions $\dot{w}_S$. Flow-Field quantities $k, \nabla T$ define the conductive heat flux vector $\dot{\mathbf{q}}$ at each surface point, with corresponding normal flux component $\dot{q}_S$. These are all associated with molecular motion.

Boundary conditions

The appropriate boundary conditions for a viscous flow at a solid surface are the *no-slip condition* on $\mathbf{V}$, and either a temperature condition or a heat-flux condition on h.

$$\mathbf{V} = \mathbf{0} \qquad \text{(on solid fixed surface)} \tag{1.39}$$

$$\text{either} \quad h = c_p T_{\text{body}} \qquad \text{(on surface with known temperature)} \tag{1.40}$$

$$\text{or} \quad \dot{\mathbf{q}} \cdot \hat{\mathbf{n}} = 0 \qquad \text{(on surface at thermal equilibrium with fluid)} \tag{1.41}$$

For the idealization of an inviscid flow, the appropriate solid surface boundary condition is the following *flow-tangency condition* on $\mathbf{V}$. No solid-surface boundary condition required for the temperature.

$$\mathbf{V} \cdot \hat{\mathbf{n}} = 0 \qquad \text{(on solid fixed surface)} \tag{1.42}$$

Definitions

ρ	density
$\boldsymbol{V}$	velocity vector
$\hat{\boldsymbol{n}}$	surface unit normal vector
$\boldsymbol{V} \cdot \hat{\boldsymbol{n}}$	(scalar) flow speed normal to surface
$\bar{\bar{\boldsymbol{\tau}}}$	(symmetric) viscous stress *tensor*
$\boldsymbol{\tau} = \bar{\bar{\boldsymbol{\tau}}} \cdot \hat{\boldsymbol{n}}$	viscous stress traction *vector* (acting *on surface*)

$$\mathbf{r} = x\hat{\mathbf{x}} + y\hat{\mathbf{y}} + z\hat{\mathbf{z}}$$
$$\mathbf{V} = u\hat{\mathbf{x}} + v\hat{\mathbf{y}} + w\hat{\mathbf{z}}$$

For steady, incompressible flow:

$$\bar{\bar{\boldsymbol{\tau}}} = \rho\nu[\boldsymbol{\nabla V} + (\boldsymbol{\nabla V})^T]/2$$

with

ν	kinematic viscosity

Representation of vector fields

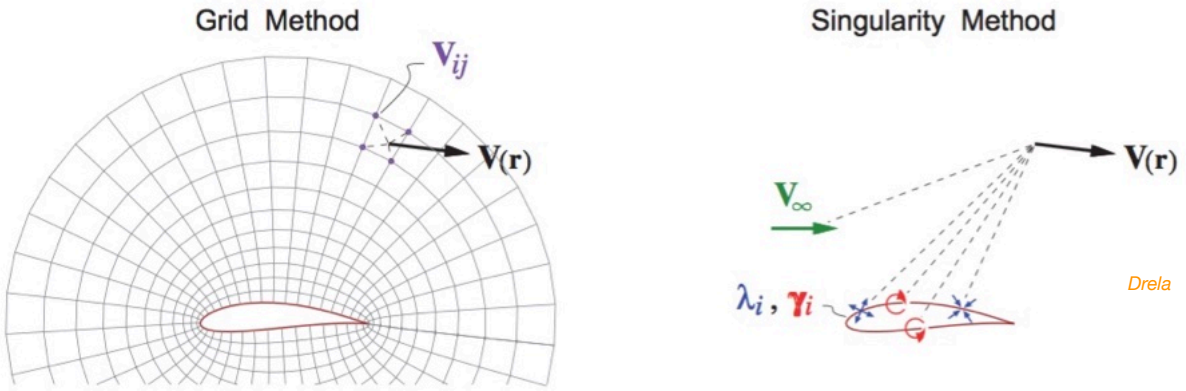

Figure 2.1: Grid and singularity methods used to represent a velocity vector field $\mathbf{V}(\mathbf{r})$.

Grid-based methods use discrete values of velocity V_{ij} at the nodes of a grid that fills the entire flow.

Suitable for solving full-PDE type problems based on the Euler or Navier–Stokes equations (conventional CFD, e.g. Ansys Fluent RANS solver).

Singularity-based methods construct the velocity field anywhere in the flow based on integration or summation of the velocity fields created by source (λ_i) and vortex sheet strengths (γ_i) defined in limited regions, typically at solid surfaces or other boundaries. These are added to the free-stream flow field (V_∞) to obtain the flow at any point.

The approach used e.g. by the Vortex Lattice and Panel methods for potential flows.
Typically many orders of magnitude faster for same accuracy than equivalent grid-based methods.

Helmholtz decomposition

Any sufficiently smooth vector field can be decomposed into the sum of a divergence-free part, and a curl-free part. Consequently we can decompose the velocity field into the sum of parts which have

1. Non-zero divergence and zero curl V_σ
2. Non-zero curl and zero divergence V_ω
3. Both zero curl and zero divergence V_b

Recall

$\sigma(\mathbf{r}) = \nabla \cdot \mathbf{V}$		Source density = div (***V***)
$\boldsymbol{\omega}(\mathbf{r}) = \nabla \times \mathbf{V}$		Vorticity = curl (***V***)
$\mathbf{V}_b$		Pure potential flow

Further, we can reconstruct the flow via volume integrals, like so:

$$\mathbf{V}(\mathbf{r}) = \mathbf{V}_\sigma + \mathbf{V}_\omega + \mathbf{V}_b$$

where

$$\mathbf{V}_\sigma(\mathbf{r}) \equiv \frac{1}{4\pi} \iiint \sigma(\mathbf{r}') \frac{\mathbf{r}-\mathbf{r}'}{|\mathbf{r}-\mathbf{r}'|^3} \, dx' \, dy' \, dz'$$

$$\mathbf{V}_\omega(\mathbf{r}) \equiv \frac{1}{4\pi} \iiint \boldsymbol{\omega}(\mathbf{r}') \times \frac{\mathbf{r}-\mathbf{r}'}{|\mathbf{r}-\mathbf{r}'|^3} \, dx' \, dy' \, dz'$$

$$\mathbf{V}_b = \mathbf{V}_\infty \quad \text{(for unbounded external flow)}$$

For incompressible flows, the source density σ(r)=0 everywhere.

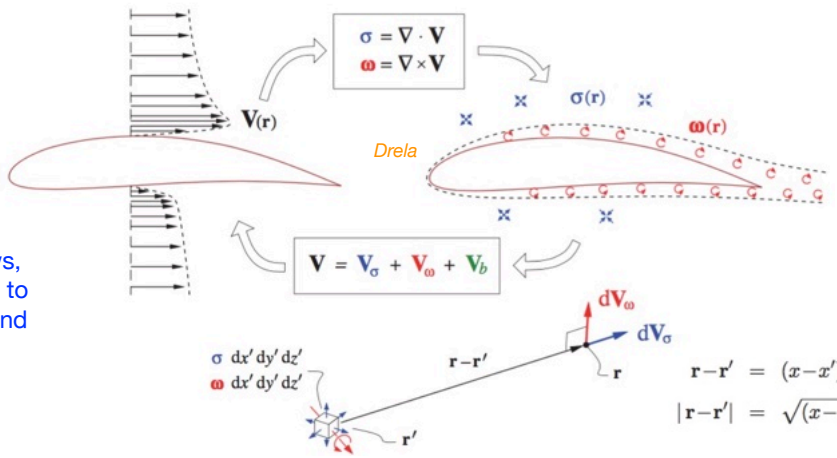

$$\mathbf{r}-\mathbf{r}' = (x-x')\,\hat{\mathbf{x}} + (y-y')\,\hat{\mathbf{y}} + (z-z')\,\hat{\mathbf{z}}$$

$$|\mathbf{r}-\mathbf{r}'| = \sqrt{(x-x')^2 + (y-y')^2 + (z-z')^2}$$

For high-Reynolds-number attached flows, vorticity ω is confined to the boundary layers and wake, and is linked to viscous stress.

Vorticity and source lumping

Standard procedure to simplify the volume integral statements

$$\mathbf{V}_\sigma(\mathbf{r}) \equiv \frac{1}{4\pi}\iiint \sigma(\mathbf{r}')\,\frac{\mathbf{r}-\mathbf{r}'}{|\mathbf{r}-\mathbf{r}'|^3}\,dx'\,dy'\,dz'$$

$$\mathbf{V}_\omega(\mathbf{r}) \equiv \frac{1}{4\pi}\iiint \boldsymbol{\omega}(\mathbf{r}')\times\frac{\mathbf{r}-\mathbf{r}'}{|\mathbf{r}-\mathbf{r}'|^3}\,dx'\,dy'\,dz'$$

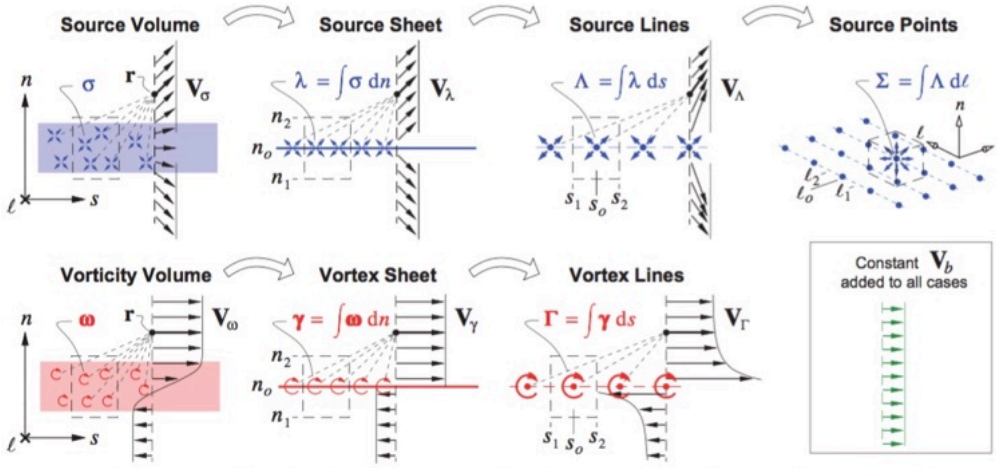

Drela

Figure 2.3: Lumping of source and vorticity volume distributions into sheets and then lines. Source lines can be further lumped into source points. The evaluation of the velocity at any field point $\mathbf{r}$ then becomes progressively simplified. Lumping is the basis of aerodynamic modeling.

Note the introduction of sheet (*s, l*) and normal (*n*) coordinates, locally orthogonal.

Volumes → sheets → lines → points

These simplifications are obtained by integrations first in *n*, then in *s*, finally (source only) in *l*.

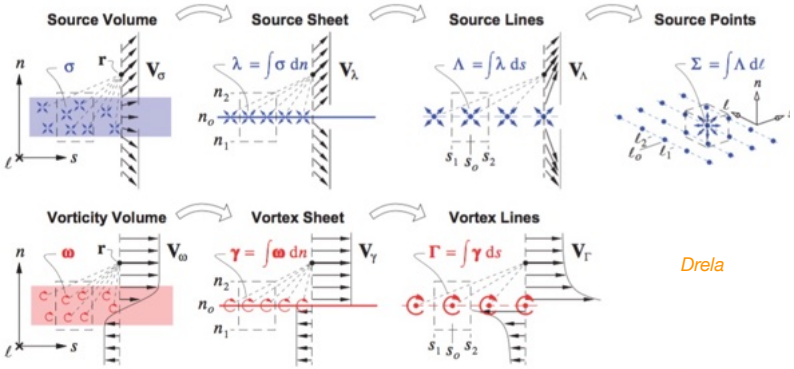

Drela

Volume→Sheet

$$\mathbf{V}_\sigma(\mathbf{r}) \simeq \mathbf{V}_\lambda(\mathbf{r}) \equiv \frac{1}{4\pi}\iint \lambda\,\frac{\mathbf{r}-\mathbf{r}'}{|\mathbf{r}-\mathbf{r}'|^3}\,ds\,d\ell \quad ; \quad \lambda(s,\ell) \equiv \int_{n_1}^{n_2}\sigma(s,\ell,n)\,dn$$

$$\mathbf{V}_\omega(\mathbf{r}) \simeq \mathbf{V}_\gamma(\mathbf{r}) \equiv \frac{1}{4\pi}\iint \boldsymbol{\gamma}\times\frac{\mathbf{r}-\mathbf{r}'}{|\mathbf{r}-\mathbf{r}'|^3}\,ds\,d\ell \quad ; \quad \boldsymbol{\gamma}(s,\ell) \equiv \int_{n_1}^{n_2}\boldsymbol{\omega}(s,\ell,n)\,dn$$

* λ, source sheet strength

* $\boldsymbol{\gamma}$, vortex sheet strength

Sheet→Line

$$\mathbf{V}_\sigma(\mathbf{r}) \simeq \mathbf{V}_\Lambda(\mathbf{r}) \equiv \sum_{\text{lines}}\frac{1}{4\pi}\int \Lambda\,\frac{\mathbf{r}-\mathbf{r}'}{|\mathbf{r}-\mathbf{r}'|^3}\,d\ell \quad ; \quad \Lambda(\ell) \equiv \int_{s_1}^{s_2}\lambda(s,\ell)\,ds$$

Λ, source line strength

$$\mathbf{V}_\omega(\mathbf{r}) \simeq \mathbf{V}_\Gamma(\mathbf{r}) \equiv \sum_{\text{lines}}\frac{1}{4\pi}\int \boldsymbol{\Gamma}\times\frac{\mathbf{r}-\mathbf{r}'}{|\mathbf{r}-\mathbf{r}'|^3}\,d\ell \quad ; \quad \boldsymbol{\Gamma}(\ell) \equiv \int_{s_1}^{s_2}\boldsymbol{\gamma}(s,\ell)\,ds$$

$\boldsymbol{\Gamma}$, vortex line strength
a.k.a. circulation

Line→Point

$$\mathbf{V}_\sigma(\mathbf{r}) \simeq \mathbf{V}_\Sigma(\mathbf{r}) \equiv \sum_{\text{points}}\frac{\Sigma}{4\pi}\,\frac{\mathbf{r}-\mathbf{r}'}{|\mathbf{r}-\mathbf{r}'|^3} \quad ; \quad \Sigma \equiv \int_{\ell_1}^{\ell_2}\Lambda(\ell)\,d\ell$$

Σ, source point strength

* NB: the limits of these integrals lie in regions where the integrand is zero.

2D forms

Vorticity, vortex sheet strength, and circulation vectors all become scalars multiplied by the page-normal unit-vector direction (below taken to be ***y***):

$$\begin{aligned}\boldsymbol{\omega} &= \omega\,\hat{\mathbf{y}}\\ \boldsymbol{\gamma} &= \gamma\,\hat{\mathbf{y}}\\ \boldsymbol{\Gamma} &= \Gamma\,\hat{\mathbf{y}}\end{aligned}$$

The velocity superposition integrals then take on the following forms in two dimensions.

$$\mathbf{V}_\sigma(\mathbf{r}) = \frac{1}{2\pi}\iint \sigma(\mathbf{r}')\,\frac{(\mathbf{r}-\mathbf{r}')}{|\mathbf{r}-\mathbf{r}'|^2}\,dx'\,dz' \tag{2.23}$$

$$\mathbf{V}_\omega(\mathbf{r}) = \frac{1}{2\pi}\iint \omega(\mathbf{r}')\,\frac{\hat{\mathbf{y}}\times(\mathbf{r}-\mathbf{r}')}{|\mathbf{r}-\mathbf{r}'|^2}\,dx'\,dz' \tag{2.24}$$

$$\mathbf{r}-\mathbf{r}' = (x-x')\,\hat{\mathbf{x}} + (z-z')\,\hat{\mathbf{z}} \tag{2.25}$$

$$|\mathbf{r}-\mathbf{r}'| = \sqrt{(x-x')^2+(z-z')^2} \tag{2.26}$$

Their simplified lumped versions follow from the same lumping procedure as in 3D. The sheet coordinates in the x-z plane are now sn, and ℓ is into the plane and parallel to y.

Line integrals along source sheets

$$\mathbf{V}_\lambda(\mathbf{r}) = \frac{1}{2\pi}\int \lambda\,\frac{(\mathbf{r}-\mathbf{r}')}{|\mathbf{r}-\mathbf{r}'|^2}\,ds \quad ; \quad \lambda(s) \equiv \int_{n_1}^{n_2}\sigma(s,n)\,dn \tag{2.27}$$

$$\mathbf{V}_\gamma(\mathbf{r}) = \frac{1}{2\pi}\int \gamma\,\frac{\hat{\mathbf{y}}\times(\mathbf{r}-\mathbf{r}')}{|\mathbf{r}-\mathbf{r}'|^2}\,ds \quad ; \quad \gamma(s) \equiv \int_{n_1}^{n_2}\omega(s,n)\,dn \tag{2.28}$$

Sums over point sources

$$\mathbf{V}_\Lambda(\mathbf{r}) = \sum_{\text{points}}\frac{\Lambda}{2\pi}\,\frac{\mathbf{r}-\mathbf{r}'}{|\mathbf{r}-\mathbf{r}'|^2} = \sum_{\text{points}}\frac{\Lambda}{2\pi}\,\frac{(x-x')\hat{\mathbf{x}}+(z-z')\hat{\mathbf{z}}}{(x-x')^2+(z-z')^2} \tag{2.29}$$

$$\mathbf{V}_\Gamma(\mathbf{r}) = \sum_{\text{points}}\frac{\Gamma}{2\pi}\,\frac{\hat{\mathbf{y}}\times(\mathbf{r}-\mathbf{r}')}{|\mathbf{r}-\mathbf{r}'|^2} = \sum_{\text{points}}\frac{\Gamma}{2\pi}\,\frac{(z-z')\hat{\mathbf{x}}-(x-x')\hat{\mathbf{z}}}{(x-x')^2+(z-z')^2} \tag{2.30}$$

3D vortex sheet divergence constraint

The components of vortex sheet strength are not entirely independent because the divergence of vorticity is zero by definition (recall vector field identity: div(curl(**A**)) = 0):

$$\nabla\cdot\boldsymbol{\omega} = \nabla\cdot(\nabla\times\mathbf{V}) = 0$$

By definition

$$\int_{n_1}^{n_2}\nabla\cdot\boldsymbol{\omega}\,dn = 0$$

$$\int_{n_1}^{n_2}\left(\frac{\partial\omega_s}{\partial s}+\frac{\partial\omega_\ell}{\partial\ell}+\frac{\partial\omega_n}{\partial n}\right)dn = 0$$

$$\frac{\partial}{\partial s}\int_{n_1}^{n_2}\omega_s\,dn + \frac{\partial}{\partial\ell}\int_{n_1}^{n_2}\omega_\ell\,dn = 0$$

Use lumping

$$\frac{\partial\gamma_s}{\partial s}+\frac{\partial\gamma_\ell}{\partial\ell} = 0 \tag{2.33}$$

$$\text{or}\qquad \widetilde{\nabla}\cdot\boldsymbol{\gamma} = 0$$

$$\text{where}\qquad \widetilde{\nabla} \equiv \hat{\mathbf{s}}\,\frac{\partial}{\partial s}+\hat{\boldsymbol{\ell}}\,\frac{\partial}{\partial\ell}$$

Notes

$\int_{n_1}^{n_2}\frac{\partial\omega_n}{\partial n}\,dn = 0$ since the vorticity is zero at n_1 and n_2.

The in-sheet (2D) divergence of ***γ*** is zero.

$\widetilde{\nabla}$ the in-sheet gradient

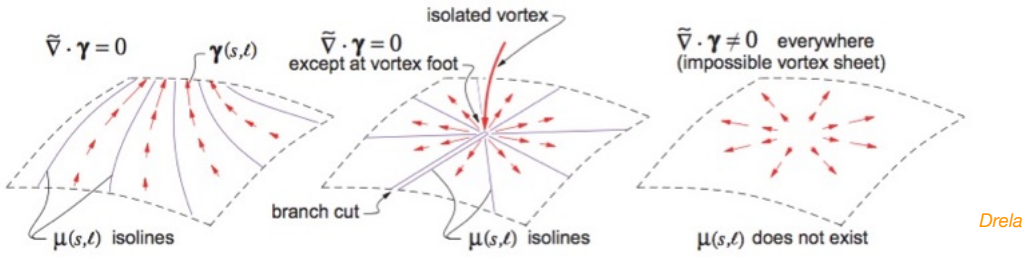

Drela

Figure 2.4: Various vortex sheet strength $\gamma_{(s,\ell)}$ distributions. Vortex normal to surface in middle case shows up as branch cut in the μ distribution associated with γ. Rightmost case is impossible.

The normal-doublet sheet strength, μ

Because of difficulties with/constraints on dealing with vortex sheets in 3D, it is standard practice to introduce the scalar *normal-doublet sheet strength* distribution μ for 3D work.

The in-sheet divergence of $\boldsymbol{\gamma}$ is zero.

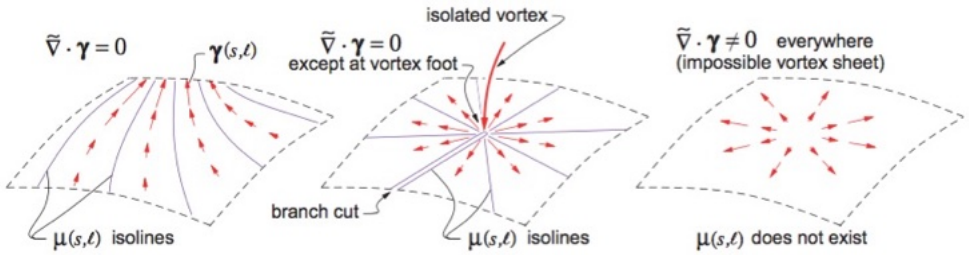

Drela

Figure 2.4: Various vortex sheet strength $\gamma(s,\ell)$ distributions. Vortex normal to surface in middle case shows up as branch cut in the μ distribution associated with γ. Rightmost case is impossible.

$$\boldsymbol{\gamma} = \hat{\mathbf{n}} \times \tilde{\nabla}\mu$$

$\boldsymbol{\gamma}$ is (vector) vortex-sheet strength

or $$\gamma_s = -\frac{\partial \mu}{\partial \ell} \quad , \quad \gamma_\ell = \frac{\partial \mu}{\partial s}$$

*Relationship between (**vector**) vortex-sheet strength and (**scalar**) doublet strength*

Note that any γ defined in this manner automatically has zero surface divergence

$$\tilde{\nabla}\cdot\boldsymbol{\gamma} = \frac{\partial \gamma_s}{\partial s} + \frac{\partial \gamma_\ell}{\partial \ell} = -\frac{\partial^2 \mu}{\partial s\,\partial \ell} + \frac{\partial^2 \mu}{\partial \ell\,\partial s} = 0$$

so that (2.33) ensures that $\omega_n = 0$. Conversely, if there is a point or line where concentrated vorticity is shed with $\omega_n \neq 0$, such as along the trailing edge of a lifting wing, then $\mu(s,\ell)$ must be discontinuous on a branch cut extending from the point, as shown in Figure 2.4. Such a branch cut must be accounted for in any calculation method which seeks to determine $\mu(s,\ell)$. In a case of a lifting wing, the branch cut is typically placed all along the trailing edge from which vorticity is shed into the otherwise irrotational flow.

The equivalence of vortex and normal-doublet sheets

$$\mathbf{V}_\mu(\mathbf{r}) = \frac{1}{4\pi}\iint \mu(s,\ell)\left[\frac{\hat{\mathbf{n}}}{|\mathbf{r}-\mathbf{r}'|^3} - 3\,\hat{\mathbf{n}}\cdot(\mathbf{r}-\mathbf{r}')\frac{\mathbf{r}-\mathbf{r}'}{|\mathbf{r}-\mathbf{r}'|^5}\right] ds\,d\ell \qquad \text{(3D)}$$

$$\mathbf{V}_\mu(\mathbf{r}) = \frac{1}{2\pi}\int \mu(s)\left[\frac{\hat{\mathbf{n}}}{|\mathbf{r}-\mathbf{r}'|^2} - 2\,\hat{\mathbf{n}}\cdot(\mathbf{r}-\mathbf{r}')\frac{\mathbf{r}-\mathbf{r}'}{|\mathbf{r}-\mathbf{r}'|^4}\right] ds \qquad \text{(2D)}$$

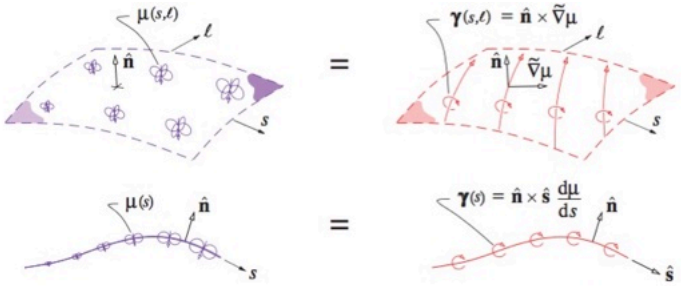

Figure 2.5: Equivalence between normal-doublet sheet and vortex sheet away from edges, for 3D and 2D cases. The doublet and vortex sheets have the same velocity fields.

Drela

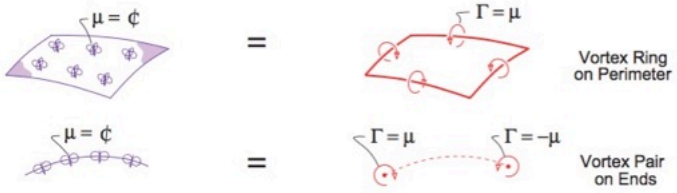

Figure 2.6: Constant-strength normal-doublet sheet with edges, and the equivalent vortex filaments, for 3D and 2D cases.

Because the elimination of the zero-divergence requirement for 3D vorticity is such a great simplification, doublet sheets are heavily favored over vortex sheets in all common 3D panel methods. However, the zero-divergence constraint does not appear in 2D, with the result that vortex sheets tend to be favored over doublet sheets in 2D panel methods.

Integral velocity / vorticity-source relations

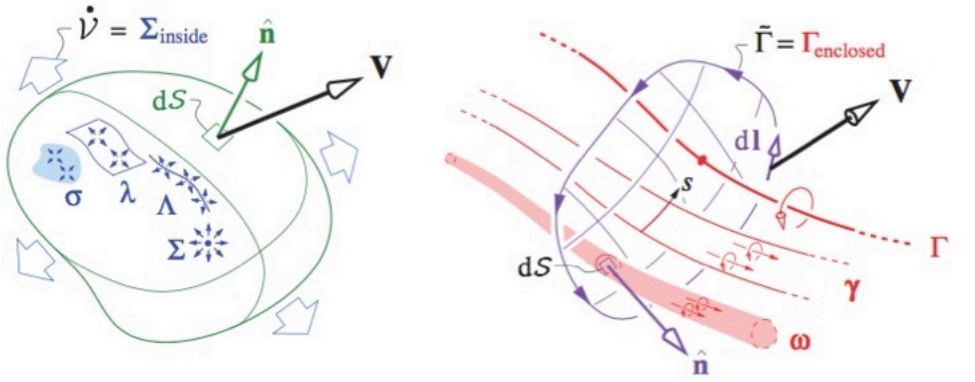

Drela

Figure 2.7: Volume outflow $\dot{\mathcal{V}}$ through closed surface (left) is equal to the total integrated source strength of all source density, sheets, filaments, and points inside. Circulation $\tilde{\Gamma}$ over closed circuit (right) is equal to the total circulation of all vorticity, vortex sheets, and vortex filaments enclosed or encircled by the circuit.

Math statements of the above:

(surface integral) (volume integral) Gauss's theorem

$$\dot{\mathcal{V}} \equiv \oiint \mathbf{V}\cdot\hat{\mathbf{n}}\, d\mathcal{S} = \iiint_{\text{inside}} \nabla\cdot\mathbf{V}\, d\mathcal{V}$$

$$= \iiint_{\text{inside}} \sigma\, dx\, dy\, dz + \iint_{\text{inside}} \lambda\, ds\, d\ell + \int_{\text{inside}} \Lambda\, d\ell + \Sigma \equiv \Sigma_{\text{inside}}$$

(line integral) (surface integral) Stokes's theorem

$$\tilde{\Gamma} \equiv \oint \mathbf{V}\cdot d\mathbf{l} = \iint_{\text{enclosed}} (\nabla\times\mathbf{V})\cdot\hat{\mathbf{n}}\, d\mathcal{S}$$

$$= \iint_{\text{enclosed}} \boldsymbol{\omega}\cdot\hat{\mathbf{n}}\, d\mathcal{S} + \int_{\text{enclosed}} \boldsymbol{\gamma}\cdot\hat{\mathbf{n}}\, ds + \Gamma \equiv \Gamma_{\text{enclosed}}$$

Recall 2D Kutta-Joukowski

$l = \rho V_\infty \Gamma$

Velocity potential integrals (3D)

2.7.1 3D potentials

Velocity potential function φ.

The velocity fields of the various types of source distributions can be expressed in terms of their velocity potentials, with $\mathbf{V}_\sigma = \nabla\varphi_\sigma$, $\mathbf{V}_\lambda = \nabla\varphi_\lambda$, etc. These are defined by the following superposition integrals.

$$\varphi_\sigma(\mathbf{r}) = \frac{1}{4\pi}\iiint \sigma(\mathbf{r}')\,\frac{-1}{|\mathbf{r}-\mathbf{r}'|}\, dx'\, dy'\, dz' \tag{2.43}$$

$$\varphi_\lambda(\mathbf{r}) = \frac{1}{4\pi}\iint \lambda(s,\ell)\,\frac{-1}{|\mathbf{r}-\mathbf{r}'|}\, ds\, d\ell \tag{2.44}$$

$$\varphi_\Lambda(\mathbf{r}) = \frac{1}{4\pi}\int \Lambda(\ell)\,\frac{-1}{|\mathbf{r}-\mathbf{r}'|}\, d\ell \tag{2.45}$$

$$\varphi_\Sigma(\mathbf{r}) = \frac{\Sigma}{4\pi}\,\frac{-1}{|\mathbf{r}-\mathbf{r}'|} \tag{2.46}$$

There is no way to explicitly give the potential of 3D vortex sheets, but it is possible to do so for 3D doublet sheets.

$$\varphi_\mu(\mathbf{r}) = \frac{1}{4\pi}\iint \mu(s,\ell)\,\frac{\hat{\mathbf{n}}\cdot(\mathbf{r}-\mathbf{r}')}{|\mathbf{r}-\mathbf{r}'|^3}\, ds\, d\ell \tag{2.47}$$

This is yet another advantage of using doublet sheets in lieu of vortex sheets.

It's again useful to note that as in the general velocity expression (2.13), each potential expression has the same form involving a kernel function. For example, (2.43) can be written as

$$\varphi_\sigma(\mathbf{r}) = \iiint \sigma(\mathbf{r}')\; K(\mathbf{r}-\mathbf{r}')\; dx'\, dy'\, dz' \tag{2.48}$$

$$K(\mathbf{r}-\mathbf{r}') = \frac{1}{4\pi}\,\frac{-1}{|\mathbf{r}-\mathbf{r}'|} \tag{2.49}$$

where now the scalar kernel function K is the potential field $\varphi(\mathbf{r})$ of a unit point source at $\mathbf{r}'$.

Velocity potential integrals (2D)

2.7.2 2D potentials

The potentials of source distributions in 2D are given below.

$$\varphi_\sigma(x,z) = \frac{1}{2\pi}\iint \sigma(\mathbf{r}')\,\ln|\mathbf{r}-\mathbf{r}'|\,\mathrm{d}x'\,\mathrm{d}z' \tag{2.50}$$

$$\varphi_\lambda(x,z) = \frac{1}{2\pi}\int \lambda(s)\,\ln|\mathbf{r}-\mathbf{r}'|\,\mathrm{d}s \tag{2.51}$$

Drela

$$\varphi_\Lambda(x,z) = \frac{\Lambda}{2\pi}\,\ln|\mathbf{r}-\mathbf{r}'| \tag{2.52}$$

Unlike in 3D, the potentials of vortex sheets and vortex filaments in 2D can be given explicitly:

$$\varphi_\omega(x,z) = \frac{1}{2\pi}\iint -\omega(\mathbf{r}')\,\arctan\left(\frac{z-z'}{x-x'}\right)\mathrm{d}x'\,\mathrm{d}z' \tag{2.53}$$

$$\varphi_\gamma(x,z) = \frac{1}{2\pi}\int -\gamma(s)\,\arctan\left(\frac{z-z'}{x-x'}\right)\mathrm{d}s \tag{2.54}$$

$$\varphi_\Gamma(x,z) = -\frac{\Gamma}{2\pi}\,\arctan\left(\frac{z-z'}{x-x'}\right) \tag{2.55}$$

For completeness we note the following, since the argument of arctan can vary past 2π: a branch cut is needed for the last equation.

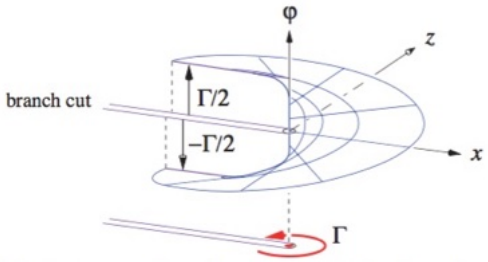

Drela

Figure 2.8: Potential of a 2D vortex located at $(x,z) = (0,0)$. Branch cut accommodates the potential jump of Γ. The sketch corresponds to a negative Γ.

Physical requirements for source distributions

Incompressible flow

$$\nabla\cdot\mathbf{V} = 0$$

$$\rightarrow \quad \sigma = \lambda = \Lambda = \Sigma = 0$$

(within flow field)

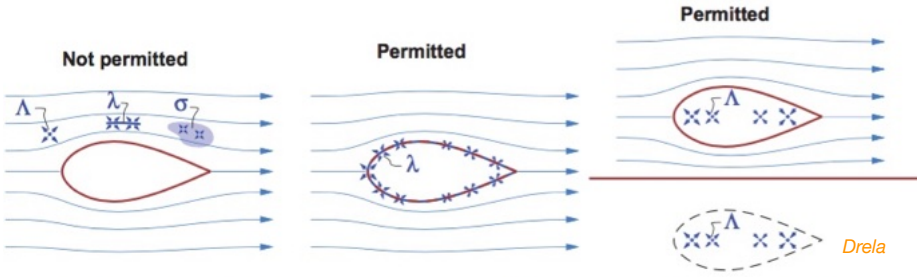

Drela

Figure 2.10: Sources within an incompressible flow-field are not permitted by continuity. Fictitious sources inside a body, on a boundary, or outside the physical flow-field are permissible.

Compressible flow

Steady flow continuity equation

$$\nabla\cdot(\rho\mathbf{V}) = 0$$

$$\rho\nabla\cdot\mathbf{V} + \nabla\rho\cdot\mathbf{V} = 0$$

$$\nabla\cdot\mathbf{V} \equiv \sigma = -\frac{1}{\rho}\nabla\rho\cdot\mathbf{V}$$

Isentropic+adiabatic case:

$$\sigma = V\frac{\nabla V}{a^2}\cdot\mathbf{V} = V^2\frac{\nabla V}{a^2}\cdot\hat{\mathbf{s}} = M^2\frac{\partial V}{\partial s}$$

NB: since σ is not confined to surface, panel methods are unsuitable for strongly compressible flows; need gridded methods.

(OK for weakly compressible.)

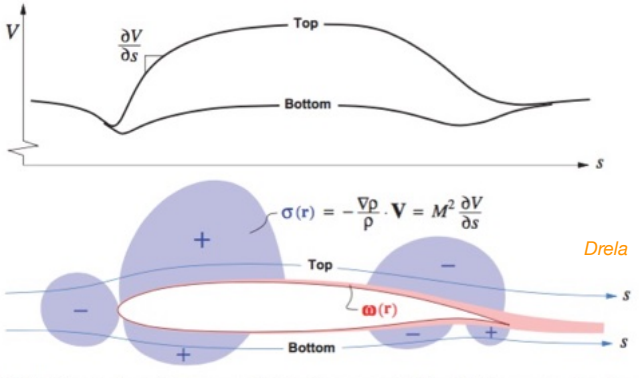

Drela

Figure 2.11: Positive and negative source distributions associated with streamwise density gradients, or the related speed gradients, near an airfoil in a compressible flow. The thin viscous vorticity layer is also shown.

Physical requirements for vorticity distributions

Provided Reynolds numbers are moderately high and flows are attached, vorticity is confined near solid surfaces and within a narrow wake:

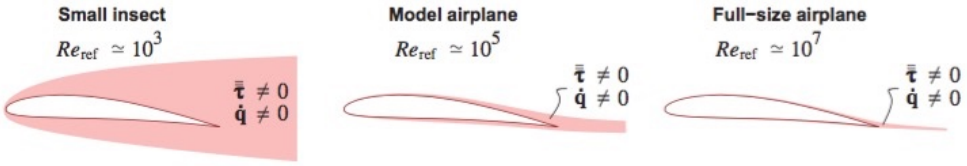

Drela

Figure 1.9: Typical aerodynamic flows with large Reynolds numbers have thin boundary layers and wakes (viscous regions) compared to the body dimension. The outer flow is effectively inviscid.

Since these requirements are often satisfied in aerodynamic applications, lumped vortex sheet models provide very effective approximations for the flow field outside boundary layers.

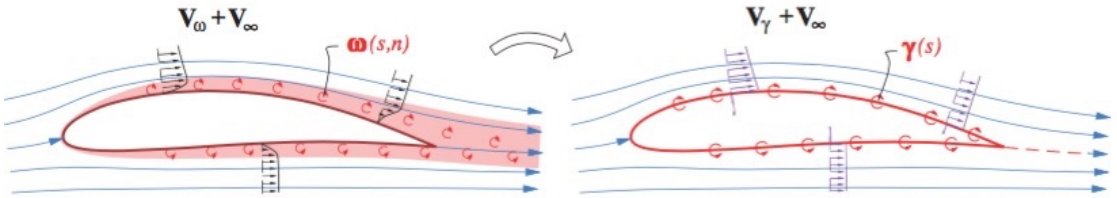

Drela

Figure 2.12: Physical vorticity $\omega(s,n)$ in thin boundary layer is lumped into vortex sheet $\gamma(s)$ placed on the airfoil surface. Outside the boundary layer, there is typically very little difference between the actual $\mathbf{V}_\omega(\mathbf{r})$ field and the approximated $\mathbf{V}_\gamma(\mathbf{r})$ field.

Note that in 2D, the trailing wake has no net vorticity.

(We will account for the influence of boundary layers and the wake using BL models, then couple that with panel-based methods. This coupling is the basis of viscous-inviscid interaction models.)

Flow field modelling with source and vortex sheets

The combination is good for low-speed aerodynamic flows (source sheets are not so good for compressible flows, though vortex sheets can still effectively represent BLs in that case).

1. Accurate for flows with thin viscous layers; vorticity lumped into vortex sheets placed on body and wake surfaces. (The standard inviscid flow approximation.) Can make effective corrections if viscous layers not thin.
2. Only the body surface and trailing wake need to be geometrically defined (simpler than a space-filling grid).
3. Numerical panel methods typically require of order 100 times less unknowns than a grid based method for equivalent accuracy.
4. If across-sheet velocity or potential jumps (ΔV, $\Delta\varphi$) are known, then source, vortex or doublet sheet strengths are also. See Drela App. B for these outcomes:

$$\lambda = \hat{\mathbf{n}} \cdot \Delta\mathbf{V}$$
$$\gamma = \hat{\mathbf{n}} \times \Delta\mathbf{V}$$
$$\mu = \Delta\varphi$$

Source sheets

Source sheets on their own are OK for inviscid low-speed flow around non-lifting bodies.

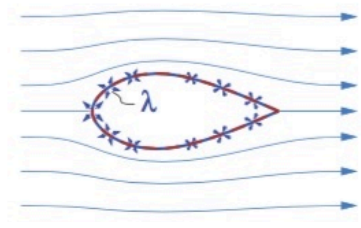

Drela

Velocity field (3D form):

$$\mathbf{V}(\mathbf{r}) = \frac{1}{4\pi} \iint \lambda(s,\ell) \frac{(\mathbf{r}-\mathbf{r}')}{|\mathbf{r}-\mathbf{r}'|^3} \, ds \, d\ell + \mathbf{V}_\infty$$

Free-slip surface BC at $\boldsymbol{r} = (s, l, 0^+)$

$$\mathbf{V}(s,\ell,0^+) \cdot \hat{\mathbf{n}}(s,\ell) = 0.$$

Equation to be solved for source sheet strength λ:

$$\frac{1}{4\pi} \iint \lambda(s,\ell) \frac{(\mathbf{r}-\mathbf{r}') \cdot \hat{\mathbf{n}}}{|\mathbf{r}-\mathbf{r}'|^3} \, ds \, d\ell = -\mathbf{V}_\infty \cdot \hat{\mathbf{n}}(s,\ell) \quad ; \quad \mathbf{r} = \mathbf{r}(s,\ell,0^+)$$

Panel methods discretise this integral equation to produce a system of equations to be solved for individual panel strengths.

Flow field modelling with source and vortex sheets

Vortex sheets Source sheets have the limitation that they cannot alone represent a lifting flow.

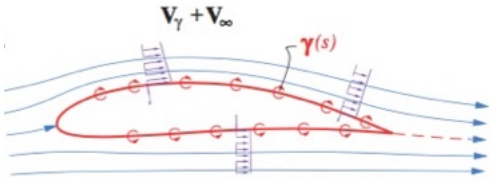

Drela

So more generally, we use vortex (or doublet) sheets.

Velocity field (2D form):

$$\mathbf{V}(\mathbf{r}) = \frac{1}{2\pi}\int \gamma(s)\,\frac{\hat{\mathbf{y}}\times(\mathbf{r}-\mathbf{r}')}{|\mathbf{r}-\mathbf{r}'|^2}\,ds + \mathbf{V}_\infty$$

Free-slip surface BC at $\boldsymbol{r} = (s, l, 0^+)$ $\mathbf{V}_{(s,\ell,0^+)}\cdot\hat{\mathbf{n}}_{(s,\ell)} = 0.$

Equation to be solved for vortex sheet strength γ (2D), again at $\boldsymbol{r}$ just outside surface:

$$\frac{1}{2\pi}\int \gamma(s)\,\frac{\hat{\mathbf{y}}\times(\mathbf{r}-\mathbf{r}')\cdot\hat{\mathbf{n}}}{|\mathbf{r}-\mathbf{r}'|^2}\,ds = -\mathbf{V}_\infty\cdot\hat{\mathbf{n}}$$

An additional constraint equation is needed to satisfy Kutta condition: $\gamma_{TE_{\text{upper}}} + \gamma_{TE_{\text{lower}}} = 0$

Again, panel methods discretise this (continuous) integral equation and Kutta condition constraint equation to produce a system of equations that can be be solved for individual panel strengths.

Non-uniqueness

Different combinations of source, vortex and freestream combinations can give the same external velocity field (though, for a lifting body, there must always be a net circulation).

Hence there are many different possible types of panel methods, based on source sheets, or vortex-doublet sheets, or both. See reference by Katz & Plotkin for an extensive overview.

Physical aspects of airfoil performance reviewed

Airfoil shape - classical definition

An airfoil is a two-dimensional section of a three-dimensional wing. Its shape is called a profile.

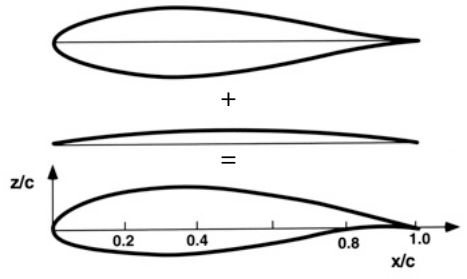

x/c	0.01	0.05	0.10	0.15	0.20	0.30	0.40	0.50	0.60	0.70	0.80	0.90	0.95	1.0
100 · z_u/c	2.6	5.6	7.9	9.3	10.4	11.8	12.1	11.3	9.7	7.5	5.1	2.5	1.3	0
100 · z_l/c	-1.3	-3.2	-4.3	-5.1	-5.6	-6.0	-5.6	-4.6	-3.2	-1.7	-0.3	0.6	0.6	0

Any airfoil profile can be decomposed into the sum of a thickness distribution and a (mean) camber line.

These two things can be changed independently and have mostly indendent effects on airfoil performance.

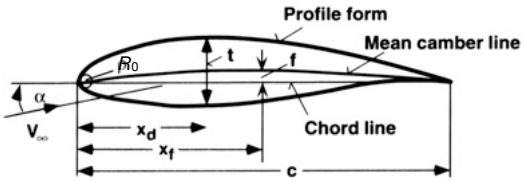

The most significant dimension of an airfoil is its chord c, and the chord line is drawn between the front and rear points of the mean camber line: these points are called the leading edge (LE) and trailing edge (TE) of the airfoil. Other leading values are usually given in dimensionless form (based on c):

The maximum thickness t and its chordwise location x_d.

The maximum camber f and its chordwise location x_f.

The nose radius R_0.

The trailing edge thickness (if finite).

The angle of attack (AOA) α is the angle made between the far-field oncoming flow velocity vector $\boldsymbol{V}_\infty$ and a reference line – often the chord line. Two significant AOAs are the zero-lift value α_0 and the stall AOA.

Another common reference line is the zero-lift line: the geometric AOA for which $C_l = 0$.

Example airfoil families

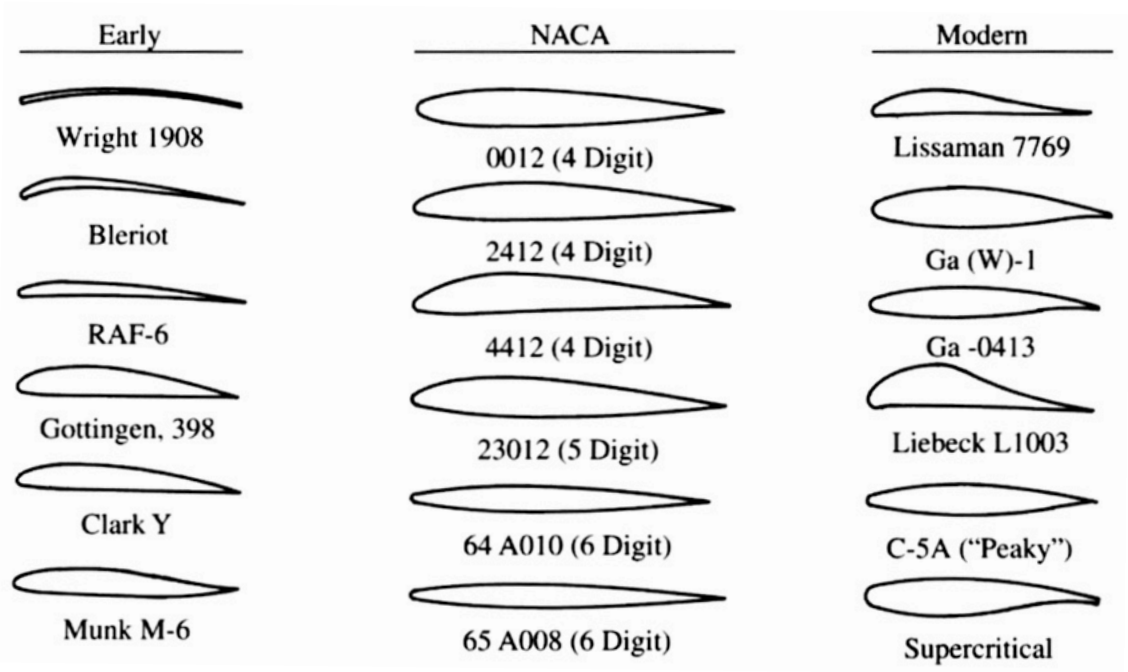

NACA airfoil series

Eastman N Jacobs

First systematic attempt to define airfoil shapes, using a rigid nomenclature and families of polynomial-type shape functions for camber and thickness.

E.g. here is the (dimensionless) thickness distribution for the NACA 4-digit series:

$$\pm y_t = \frac{t}{0.20}\left(0.29690\sqrt{x} - 0.12600x - 0.35160x^2 + 0.28430x^3 - 0.10150x^4\right)$$

1. NACA 4-digit series:

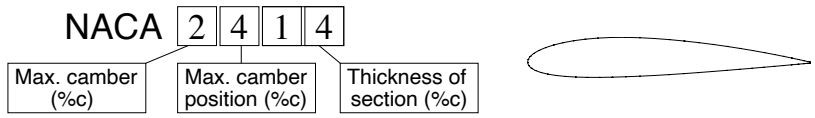

2. NACA 5-digit series:

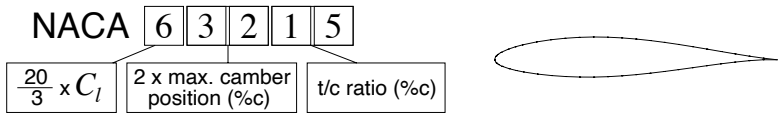

3. NACA 6-series (confusingly, the third digit can be a subscript, and sometimes omitted!):

See Abbott & von Doenhoff for the full nomenclature.

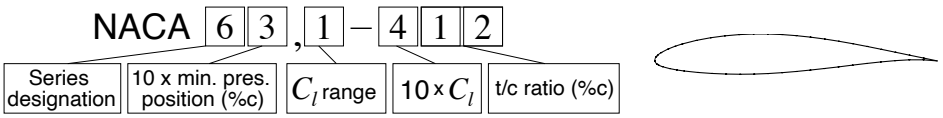

Airfoil shape: modern definition

Shape is defined through a set of control points and local shape functions: $\boldsymbol{x} = \sum_{i=1}^{N} \boldsymbol{x}_i N_i(s)$

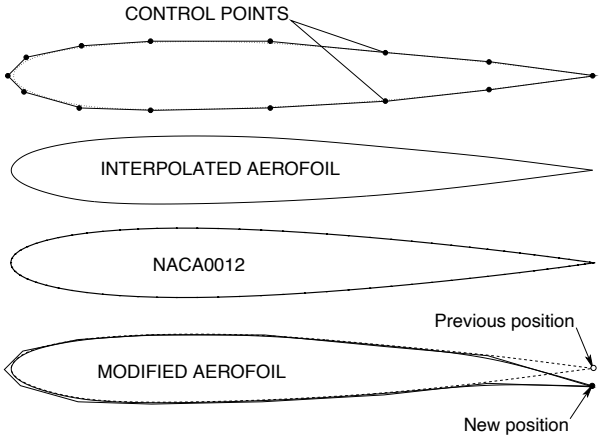

This approach allows us much more freedom in design, especially when we need to affect flow over the top and bottom of the airfoil separately (e.g. for transcritical flows with local shocks).

But it also makes it more difficult to choose an airfoil ‘off the shelf’.

Representative airfoil Reynolds numbers, $Re=V_\infty c/\nu$

1. Airfoil performance is quite heavily affected by Reynolds number, especially say below a few million.
2. Airfoil performance (L/D) degrades as Re reduces and boundary layers become relatively thicker.
3. Since it's typical for high Reynolds and Mach numbers to go together, the attention in airfoil design for high-Re aircraft tends to shift from controlling boundary layer to shock wave behaviour.

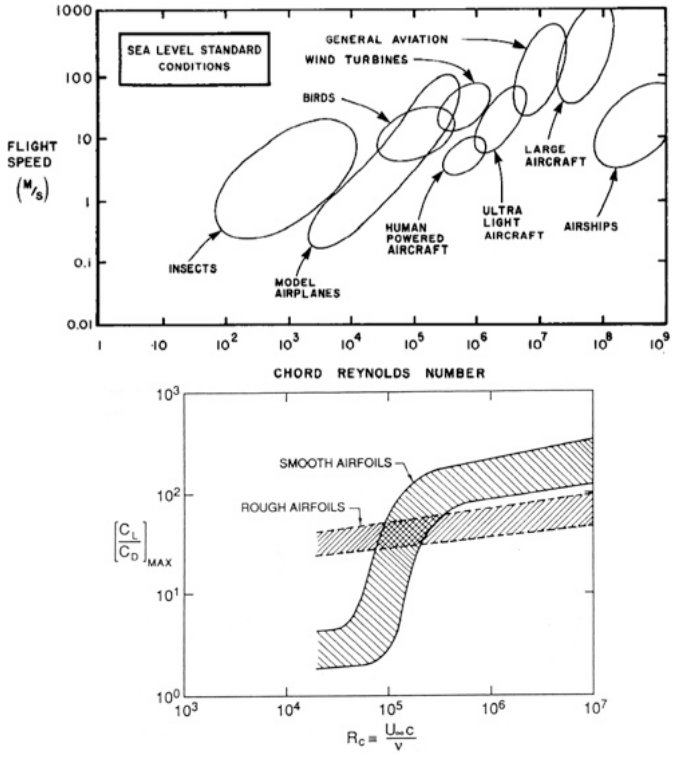

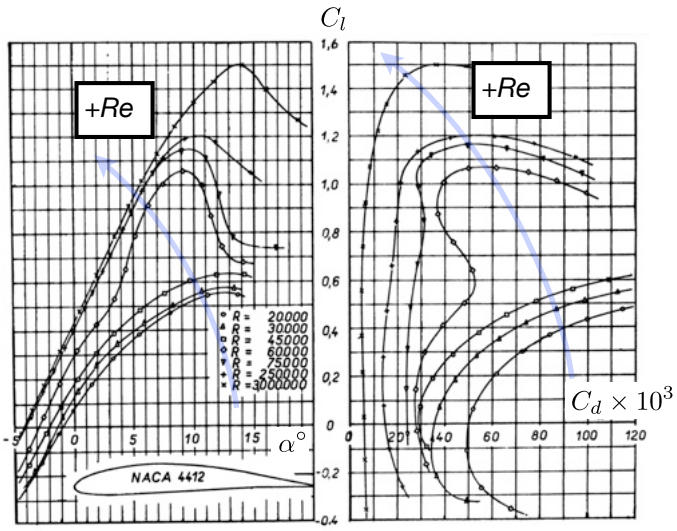

Forces on airfoils

Local: pressure and skin friction (tractions)

Unit normal and tangent vectors.

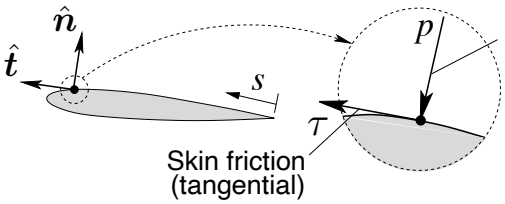

Surface tractions.

NB: one can show that the normal traction is caused only by pressure and the tangential traction only by viscous stress.

$$\boldsymbol{\tau} = \tau\hat{\boldsymbol{t}}$$

Global: lift, drag, and pitching moment

$$\boldsymbol{R} = \int_0^l (-p\hat{\boldsymbol{n}} + \tau\hat{\boldsymbol{t}})\,\mathrm{d}s \qquad \boldsymbol{M}_{\boldsymbol{x}_0} = \int_0^l (\boldsymbol{x}(s) - \boldsymbol{x}_0) \times (-p\hat{\boldsymbol{n}} + \tau\hat{\boldsymbol{t}})\,\mathrm{d}s \quad (\boldsymbol{x}_0 \text{ is arbitrary})$$

Lift and drag are the reaction force resolved normal and tangential to oncoming flow direction:

$$L = R_x \cos\alpha + R_y \sin\alpha \qquad D = -R_x \sin\alpha + R_y \cos\alpha$$

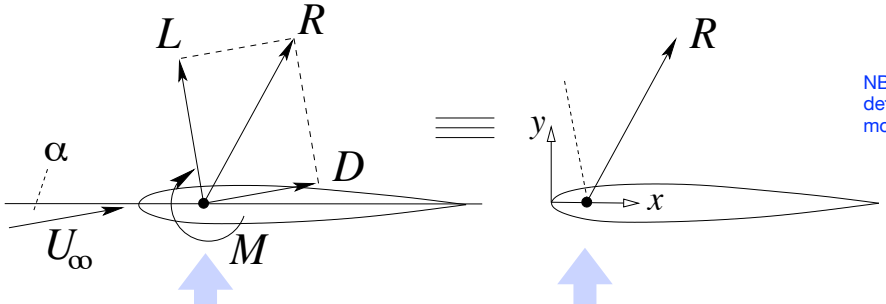

NB: by convention (and definition above) a +ve moment twists nose up.

Aerodynamic centre close to c/4: moment is constant with α.

Centre of pressure (no moment).

Aerodynamic coefficients

	Local/sectional	Global/wing/vehicle	
Pressure coefficient	$C_p = \frac{p - p_\infty}{\frac{1}{2}\rho V_\infty^2}$		NB: by convention, lower-case subscripts (C_l etc.) denote sectional (2D) values while upper-case subscripts (C_L etc.) denote whole-aircraft (or 3D) values.
Skin friction coefficient	$C_f = \frac{\sigma}{\frac{1}{2}\rho V_\infty^2}$		
Lift coefficient	$C_l = \frac{L}{\frac{1}{2}\rho V_\infty^2 c}$	$C_L = \frac{L}{\frac{1}{2}\rho V_\infty^2 S}$	S is the wing area
Drag coefficient	$C_d = \frac{D}{\frac{1}{2}\rho V_\infty^2 c}$	$C_D = \frac{D}{\frac{1}{2}\rho V_\infty^2 S}$	
Moment coefficient	$C_m = \frac{M}{\frac{1}{2}\rho V_\infty^2 c^2}$	$C_M = \frac{M}{\frac{1}{2}\rho V_\infty^2 S\bar{c}}$	$\bar{c}$ is the mean aerodynamic chord (defined later)

↑ forces and moments here are per unit span length.

Dimensional analysis shows that for steady flow

$$C_i = \text{function}(\text{shape}, M_\infty, Re); \quad i = p, f, l, d, m$$

$$M_\infty = V_\infty / a$$
$$Re = \rho c V_\infty / \mu = c V_\infty / \nu$$

Pressure distributions and pressure coefficient — 1

The pressure coefficient C_p is a convenient dimensionless way of describing the pressure on a surface, relative to the ambient pressure p_∞.

$$C_p = \frac{p - p_\infty}{\frac{1}{2}\rho V_\infty^2}$$

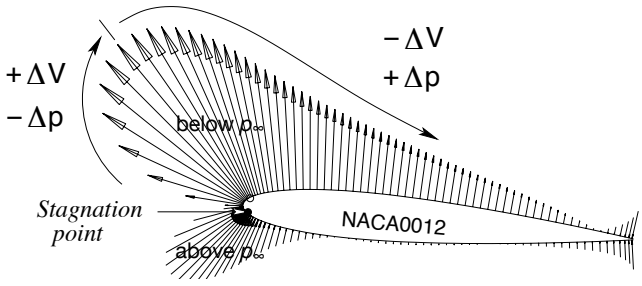

Note that by convention the pressure coefficient is plotted inverted (suction to top) as a function of chord position. This plot reveals a great deal of information about flow behaviour.

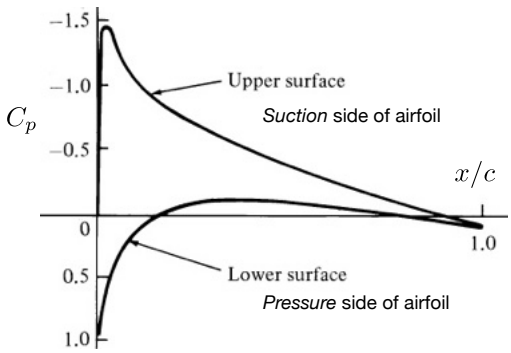

Using Bernoulli's equation we can relate C_p to the local velocity just outside the boundary layer, U_e (since pressures are typically almost invariant across a boundary layer).

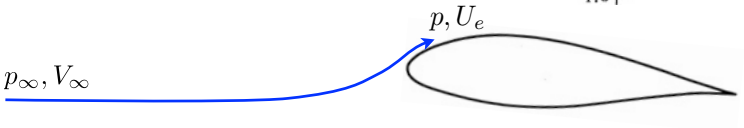

$$\frac{1}{2}\rho V_\infty^2 + p_\infty = \frac{1}{2}\rho U_e^2 + p \quad \text{rearrange} \Rightarrow \quad U_e/V_\infty = \sqrt{1 - C_p} \quad \text{alternatively} \quad 1 - C_p = \frac{U_e^2}{V_\infty^2}$$

Pressure distributions and pressure coefficient — 2

1. At a stagnation point, U_e=0 and C_p=1, its maximum value.
2. Where C_p=0, U_e=V_∞.
3. Where C_p=constant with x/c, the flow speed is constant.
4. The flow accelerates where -C_p increases with x/c (a favourable pressure gradient for boundary layers).
5. Conversely the flow deaccelerates where -C_p decreases with x/c (an unfavourable or adverse pressure gradient).
6. Small local variations/wiggles in a C_p curve signal local flow separations — may be a sign of trouble (BUT if present in an inviscid analysis usually a sign of 'noisy' airfoil coordinate data).
7. Regions where there is the greatest C_p differential between the suction and pressure sides of an airfoil provide the greatest lift contribution (do the most work).
8. The area contained by the C_p vs. x/c distribution equals the coefficient of lift C_l (this is only strictly true at zero angle of attack). Obviously, the greater the area contained, the greater C_l.
9. Surface pressure distributions are of course readily obtained in experiments.

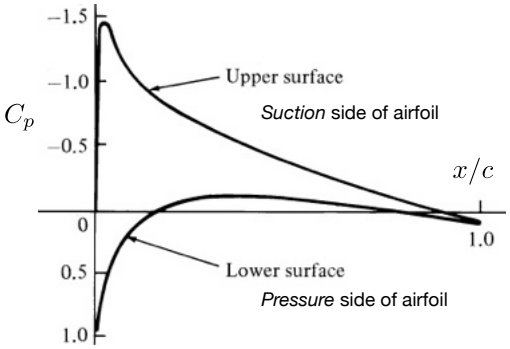

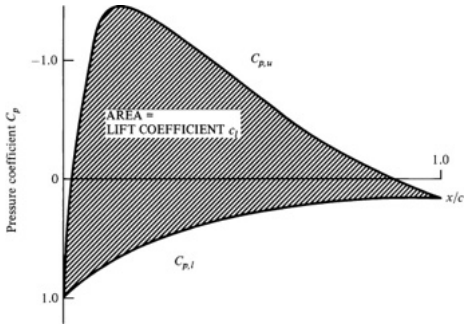

Pressure distributions and pressure coefficient — 3

1. The local surface curvature strongly influences C_p.

Conservation of momentum in direction normal to streamline: balance pressure gradient & centripetal acceleration (ignoring effect of viscosity) gives

$$\frac{\partial p}{\partial n} = \frac{\rho V^2}{R}$$

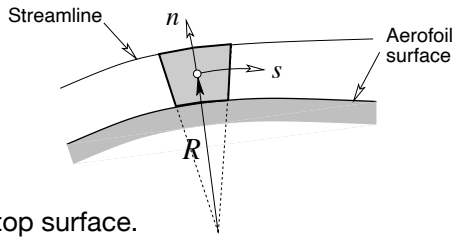

Consequences

a) Curvature of streamlines affects pressure and hence lift.
b) Increases in curvature raise suction (and local speed) on top surface.

2. The angle of attack α influences C_p (hence C_l, and local velocities too).

Note that if say -C_p=3 then the local velocity U_e=2×V_∞.

$$1 - C_p = \frac{U_e^2}{V_\infty^2}$$

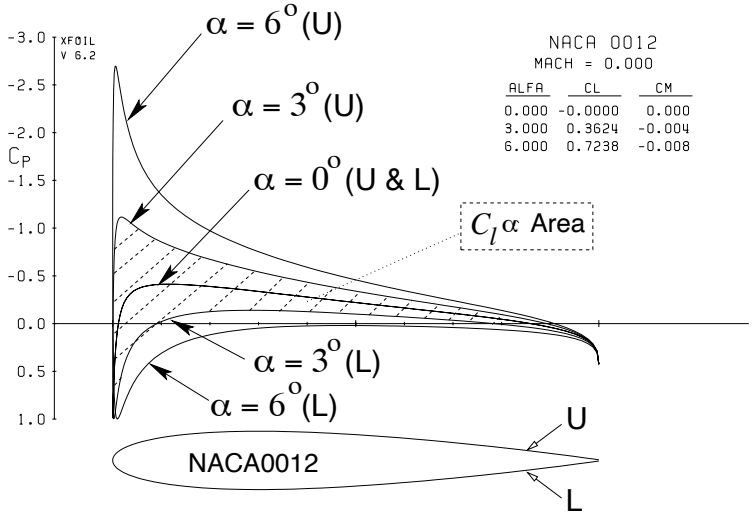

Pressure distributions and pressure coefficient — 4

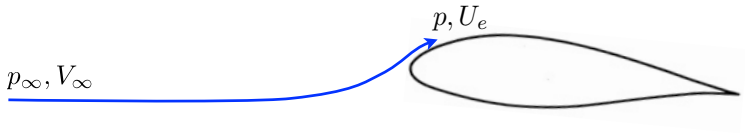

$\frac{1}{2}\rho V_\infty^2 + p_\infty = \frac{1}{2}\rho U_e^2 + p$ rearrange ⇒ $U_e/V_\infty = \sqrt{1 - C_p}$ alternatively $1 - C_p = \frac{U_e^2}{V_\infty^2}$

Reminder that (at least on the assumption in inviscid flow and accuracy of Bernoulli's equation) the information contained in plots of C_p, $(U_e/V_\infty)^2$ or (U_e/V_∞) vs x/c all present essentially the same information: the local flow speed near the surface of the airfoil relative to the freestream speed:

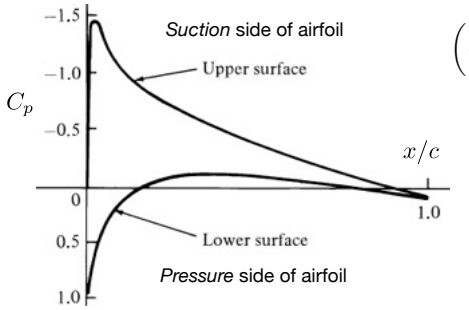

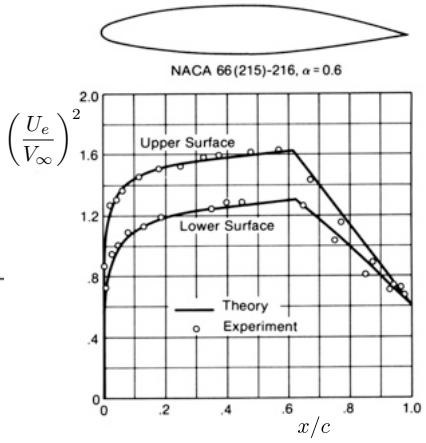

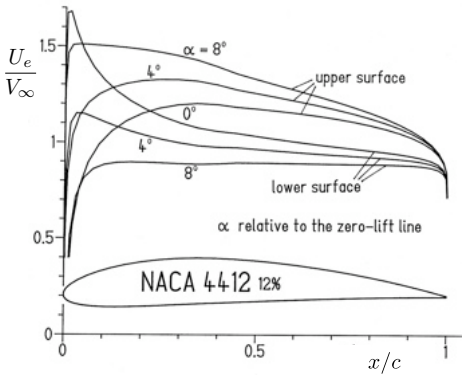

Influence of C_p on boundary layers — 1

1. Boundary layers typically start out laminar at stagnation/LE, unless externally turbulated/tripped.

2. With zero pressure gradient, flat-plate boundary layers are convectively unstable and transition to turbulence at a local Re_x that depends on surface roughness and free-stream turbulence level.

This plot is of integrated, not local, skin friction coefficient. I.e. it represents the total drag per unit span.

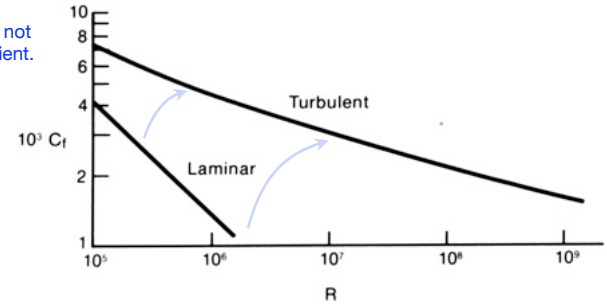

Indicative transition *Re* range approximates typical subsonic wing Reynolds numbers.

Turbulent skin friction/drag increasingly greater than laminar as *Re* increases.

3. Favourable (pressure decreasing/external speed increasing) and unfavourable (pressure increasing/external speed decreasing) pressure gradients <u>strongly affect boundary layer shape</u>.

velocity as proportion of external

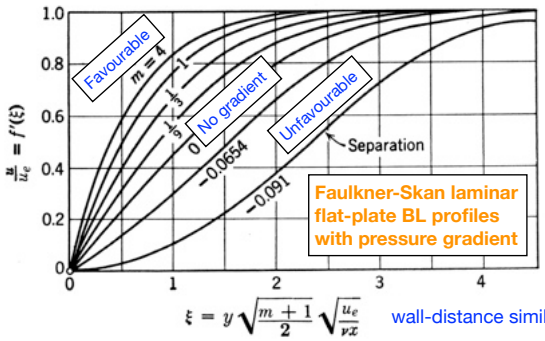

wall-distance similarity parameter

Separation corresponds to inception of reversing flow at the wall: sufficiently unfavourable pressure gradients will force flow to separate from the wall.

Influence of C_p on boundary layers — 2

4. Favourable (pressure decreasing/external speed increasing) and unfavourable (pressure increasing/external speed decreasing) pressure gradients strongly affect boundary layer stability and transition to turbulence. Initial 2D wavy disturbances are known as Tollmein-Schlichting (T-S) waves.

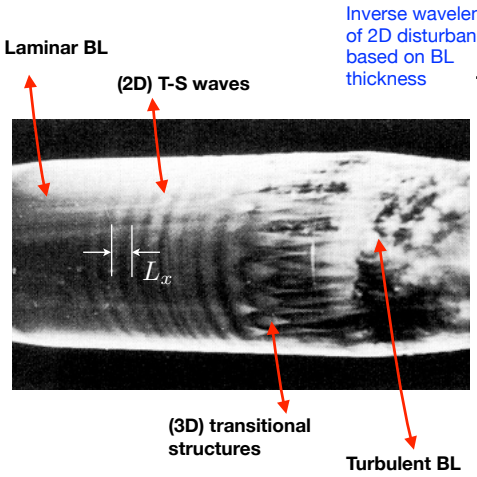

Inverse wavelength of 2D disturbance based on BL thickness

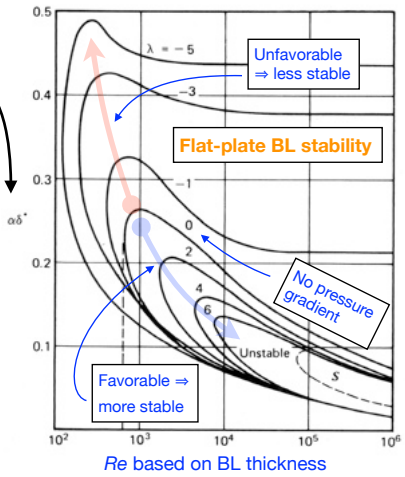

2D boundary layers are unstable inside loops/curves on this plot.

Unfavourable gradients expand enclosed region of instability (more unstable) and vice versa.

Note that for zero and favourable pressure gradients, BLs are unstable only with a certain range of downstream distances.

$\alpha = 2\pi/L_x$
$\delta^* = \text{BL displacement thickness}$
$\lambda = (\delta^2/\nu)\mathrm{d}u_e/\mathrm{d}x$

5. Separated shear layers are even more unstable than adverse-gradient attached/boundary layers.

6. Because boundary layers are relatively thin, airfoil surface curvature is relatively small, allowing airfoil BLs to be analysed with the same tools developed for flat plate BLs.

7. Although turbulent BLs produce more skin friction drag, they are also better able to resist flow separation in the presence of an adverse pressure gradient — so promoting transition may reduce overall drag. In effect we exchange increased skin friction drag for reduced profile/pressure drag.

Influence of C_p on boundary layers — 3

8. Unfavourable pressure gradients promote separation because the pressure is almost invariant in the wall-normal direction. Slower-moving layers come to rest and reverse direction sooner.

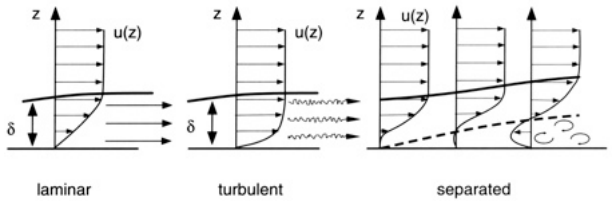

For inviscid flow along a streamline (coord. *s*) we can derive

$$\frac{\partial V}{\partial s} = -\frac{1}{\rho V}\frac{\partial p}{\partial s}$$

⇒ slow flow slows faster in an adverse pressure gradient.

9. Separated flow may reattach to form a separation bubble — indicated in C_p distribution.

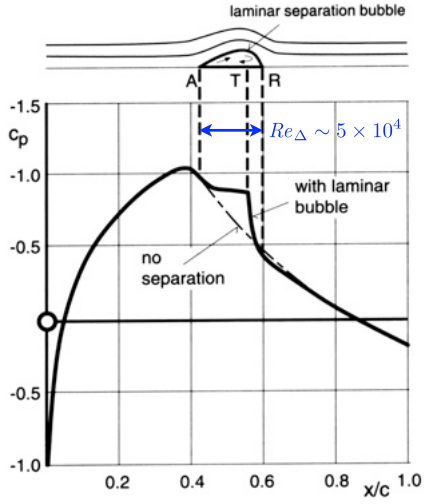

Separation bubbles may be laminar or turbulent depending on the upstream flow but often they are also a location of transition: separated shear layers are more unstable than attached ones (↑ transition) and once turbulent will grow cross-flow less rapidly (↑ attachment) and entrain external fluid (↑ reattachment).

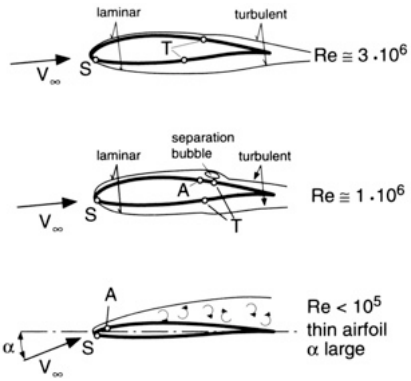

Whether a bubble or transition occurs first depends on *Re* as well as C_p.

If adverse pressure gradient is sufficiently strong the flow may stay detached (stall).

Influence of C_p on boundary layers — 4

10. A shock wave (rapid compression) provides an extremely adverse pressure gradient and can produce immediate flow transition or separation. Especially the latter leads to a rapid rise in profile drag with M_∞ in transonic flows.

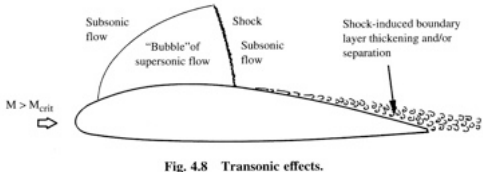

Fig. 4.8 Transonic effects.

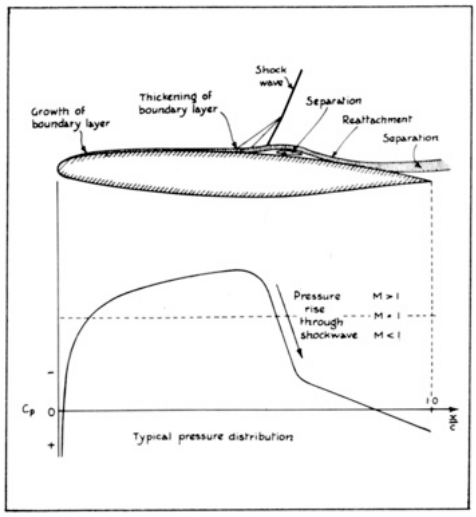

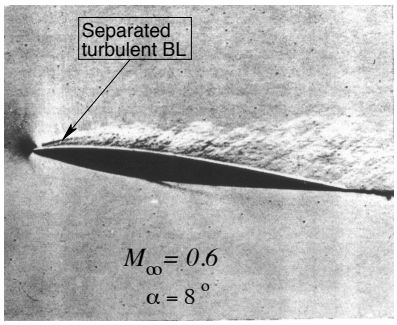

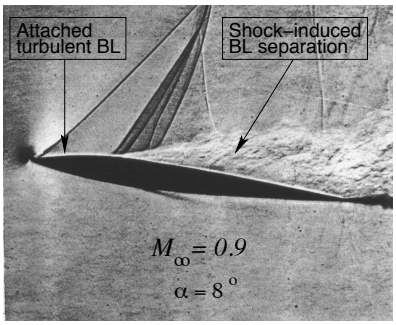

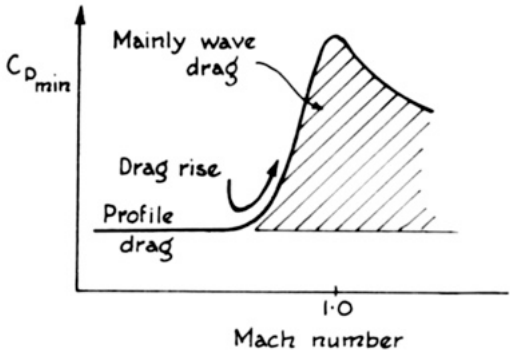

Flow separation and stall — 1

1. Stall is defined to be the maximum on the C_l-α curve and is associated with onset of complete flow separation from the suction surface. Depending on conditions, it may occur in a number of ways:

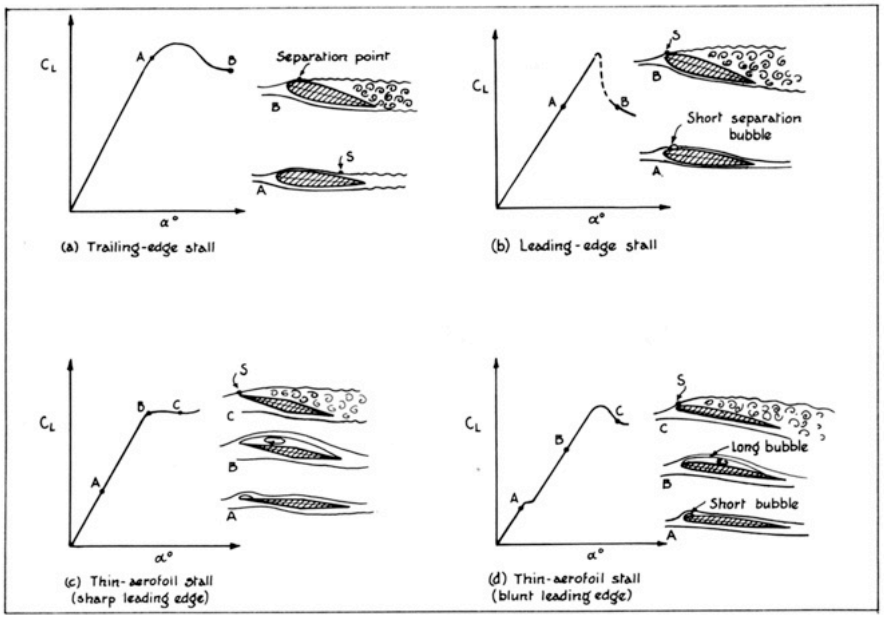

2. A very ‘sharp’ or sudden stall is generally undesirable because it is difficult for pilots to anticipate.

Flow separation and stall — 2

3. Stall is dangerous as a considerable loss of altitude may be required for recovery, and control is lost.

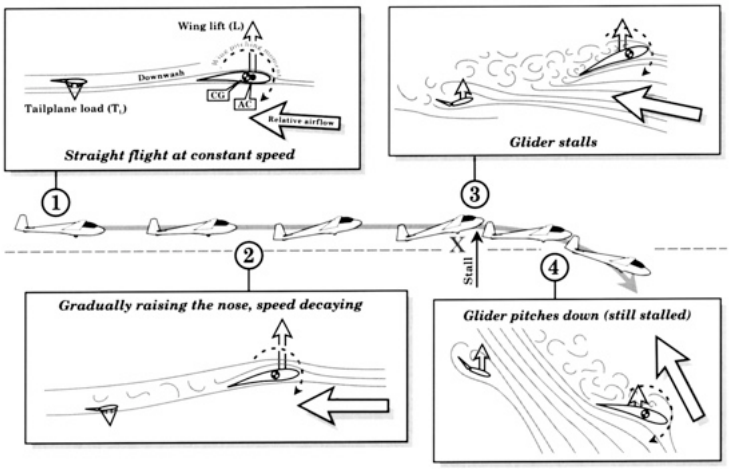

4. In addition there is the shape of the C_m-α curve to be considered. For stable stall recovery, it is desirable for the aircraft to tend to pitch nose-down i.e. for C_m to become more negative, post-stall.

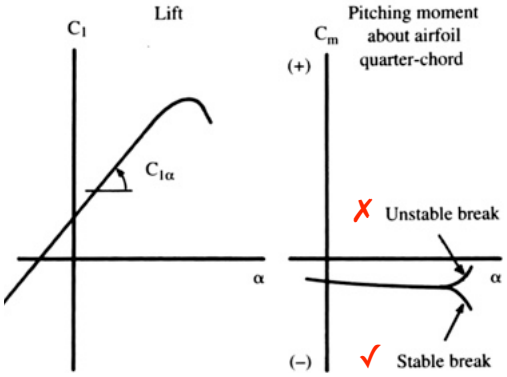

Sectional force and moment curves

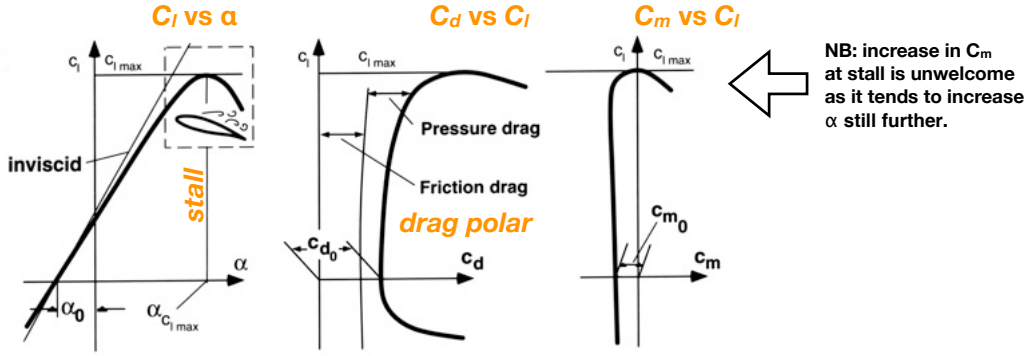

1. Note zero-lift angle of attack α_0, and the associated drag and moment coefficients (C_{d0}, C_{m0}).
2. The most important features of the C_l vs α curve are α_0, $C_{l\max}$ and α_{stall}, and lift curve slope $\partial C_l/\partial\alpha$.
3. Typically (for a positively cambered airfoil) α_0 is negative, as is C_{m0}.

The ideal that we aim for in airfoil design or selection

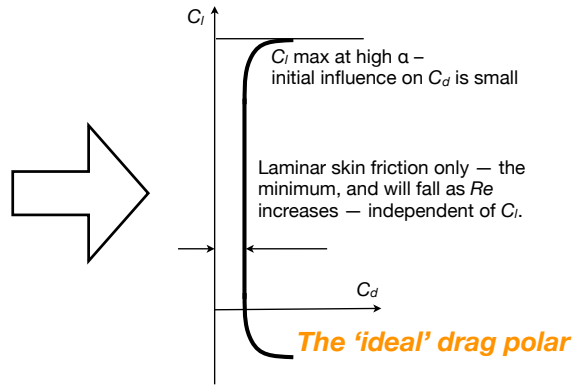

Forces and moments on airfoils

Reminder: the reference line for AOA might instead be the zero-lift line.

We can integrate the normal and tangential tractions around the periphery of the airfoil to obtain a an equivalent force *R*, and also a twisting moment M_x.

R is independent of location but M_x is associated with a given reference chordwise position *x*.

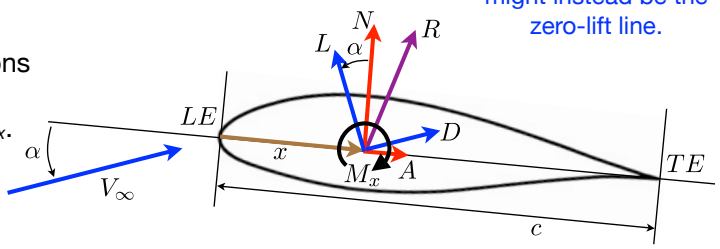

Note M_x is taken positive for LE nose up.

The force *R* can be decomposed into orthogonal components, either normal and tangential to the chord line (components *N* and *A*), or normal and tangential to the relative wind direction (components *L* and *D*).

Working with coefficients C_n, C_a, C_l, C_d, C_{mx} where e.g. $C_n = \frac{N}{\frac{1}{2}\rho V_\infty^2}$ $C_{mx} = \frac{N}{\frac{1}{2}\rho V_\infty^2 c}$

$$C_l = C_n \cos\alpha - C_a \sin\alpha \qquad C_d = C_a \cos\alpha + C_n \sin\alpha$$

or

$$C_n = C_l \cos\alpha + C_d \sin\alpha \qquad C_a = C_d \cos\alpha - C_l \sin\alpha$$

Supposing we wanted to take the moment about the LE instead (for example), i.e. C_{mLE}, given C_{mx}. Then

$$C_{m_{LE}} = C_{mx} - \frac{x}{c} C_n$$

Now we consider the two most aerodynamically significant chordwise locations:

centre of pressure x_{cp} = location for which moment is zero.

aerodynamic centre x_{ac} = location for which moment does not change with α (or e.g. *L*).

Forces and moments on airfoils

centre of pressure x_{cp} = location for which moment is zero.

$$C_{m_{LE}} = C_{mx} - \frac{x}{c} C_n = 0 - \frac{x_{cp}}{c} C_n \qquad \text{or} \qquad \frac{x_{cp}}{c} = \frac{x}{c} - \frac{C_{mx}}{C_n}$$

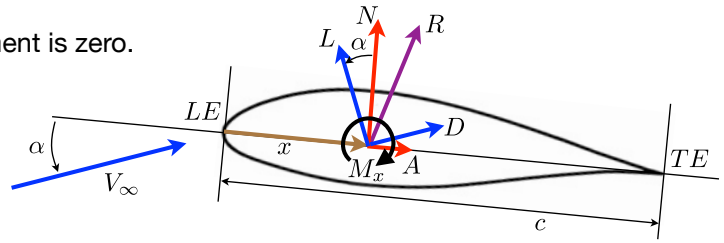

So if we know C_{mx} for a given *x* we can compute x_{cp}/c.

aerodynamic centre x_{ac} = location for which moment does not change with α (or e.g. *L*).

$$C_{m_{LE}} = C_{mx} - \frac{x}{c} C_n = C_{m_{ac}} - \frac{x_{ac}}{c} C_n \qquad \text{or} \qquad C_{m_{ac}} = C_{mx} + \left(\frac{x_{ac}}{c} - \frac{x}{c}\right) C_n$$

then $$\frac{\partial C_{m_{ac}}}{\partial \alpha} = \frac{\partial C_{mx}}{\partial \alpha} + \left(\frac{x_{ac}}{c} - \frac{x}{c}\right) \frac{\partial C_n}{\partial \alpha} = 0 \qquad \text{or} \qquad \frac{\partial C_{mx}}{\partial \alpha} \Big/ \frac{\partial C_n}{\partial \alpha} + \left(\frac{x_{ac}}{c} - \frac{x}{c}\right) = 0$$

$$\frac{x_{ac}}{c} = \frac{x}{c} - \frac{\partial C_{mx}}{\partial \alpha} \Big/ \frac{\partial C_n}{\partial \alpha} = \frac{x}{c} - \frac{\partial C_{mx}}{\partial C_n}$$

So if we know $\partial C_{mx}/\partial\alpha$ for a given *x*, as well as $\partial C_n/\partial\alpha$, we can compute x_{ac}/c.

Recall $C_n = C_l \cos\alpha + C_d \sin\alpha$ so $\frac{\partial C_n}{\partial \alpha} = \left(\frac{\partial C_l}{\partial \alpha} + C_d\right)\cos\alpha + \left(\frac{\partial C_d}{\partial \alpha} - C_l\right)\sin\alpha$

Typically α is small in which case $\frac{\partial C_n}{\partial \alpha} \approx \frac{\partial C_l}{\partial \alpha}$ and $\frac{\partial C_{mx}}{\partial C_n} \approx \frac{\partial C_{mx}}{\partial C_l}$

Forces and moments on airfoils

$$\frac{x_{cp}}{c} = \frac{x}{c} - \frac{C_{mx}}{C_l \cos\alpha + C_d \sin\alpha}$$

$$\frac{x_{ac}}{c} = \frac{x}{c} - \frac{\partial C_{mx}/\partial\alpha}{\left(\frac{\partial C_l}{\partial\alpha} + C_d\right)\cos\alpha + \left(\frac{\partial C_d}{\partial\alpha} - C_l\right)\sin\alpha}$$

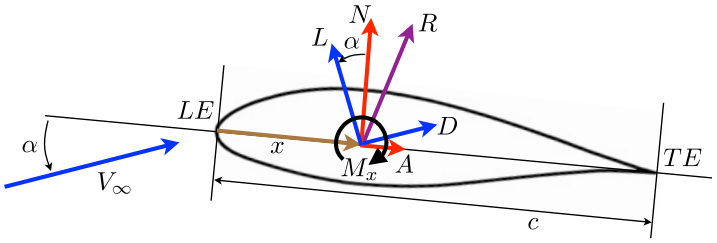

Typically, for a positively cambered airfoil, $C_{mac} < 0$ and $C_l = 0$ occurs for $\alpha < 0$.

Note that x_{cp} varies significantly with α, while x_{ac} is almost totally independent of α.

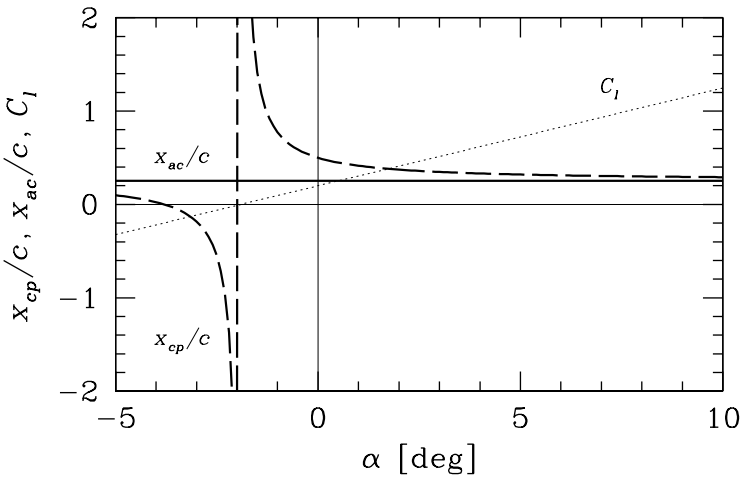

Typically with airfoil data, C_m is given for x/c = 1/4 if not otherwise stated – for many airfoils this is within a few percent of the aerodynamic centre.

Forces and moments on airfoils

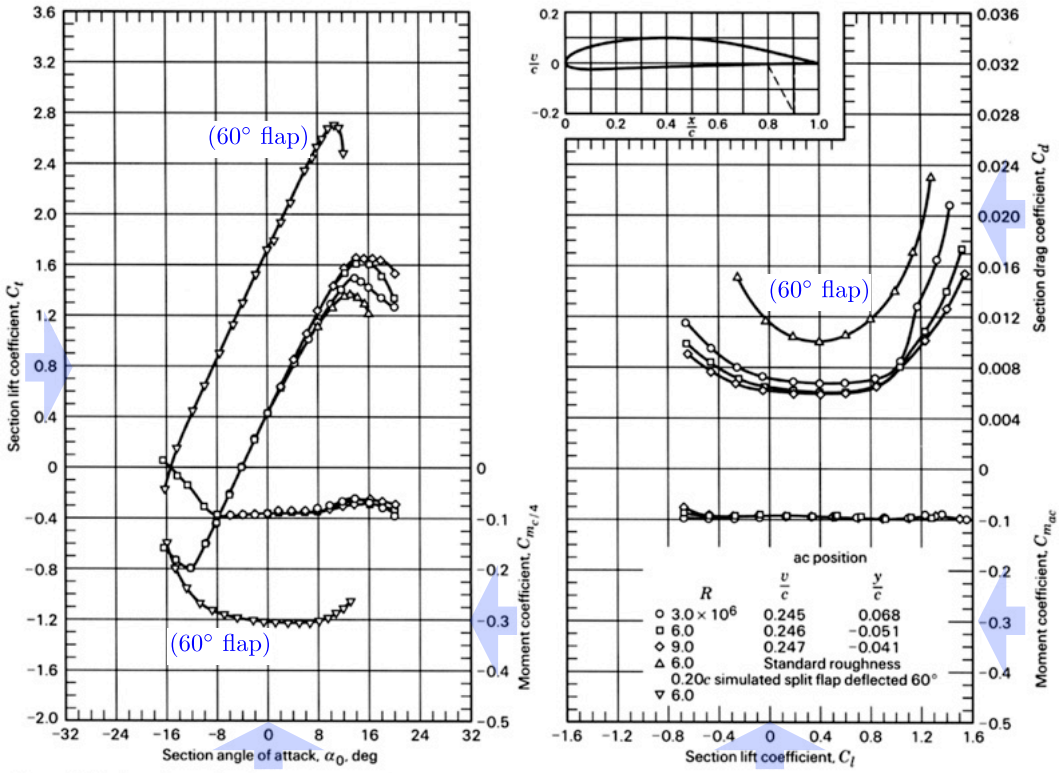

Figure 3.7 Aerodynamic characteristics of the NACA 4412 airfoil.

Influence of airfoil shape: camber distribution — 1

Generalizations:

Camber distribution is typically chosen to generate minimum drag at a desired C_l, and/or C_{lmax}.

Thickness distribution is typically chosen to influence boundary layer and shock-wave behaviour.

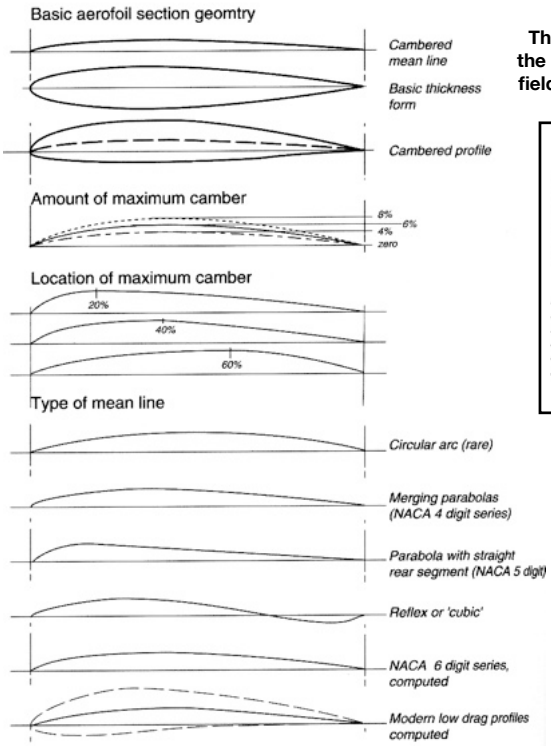

The basic idea is to streamline the mean camber line to the flow field at the design lift coefficient.

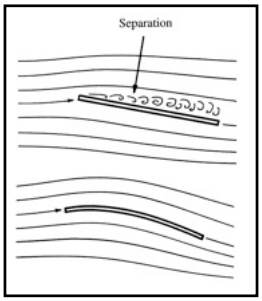

Increasing C_{lmax}:

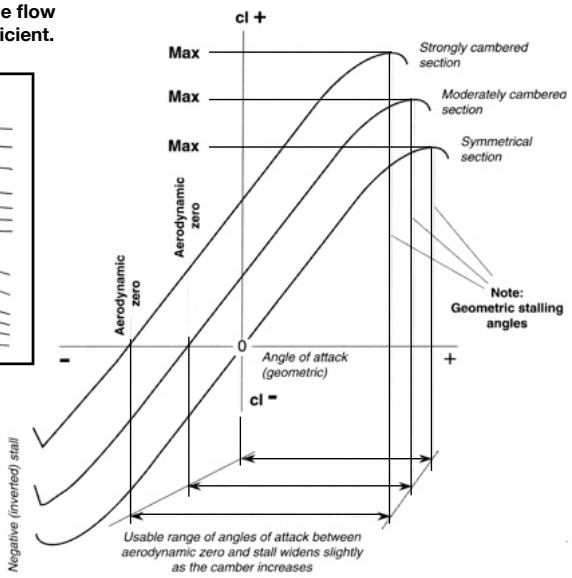

Effect on C_l-α of increasing camber:
1. α_0 reduces;
2. C_{lmax} increases;
3. Useable range of α increases.

Influence of airfoil shape: camber distribution— 2

Minimizing C_d at design C_l:

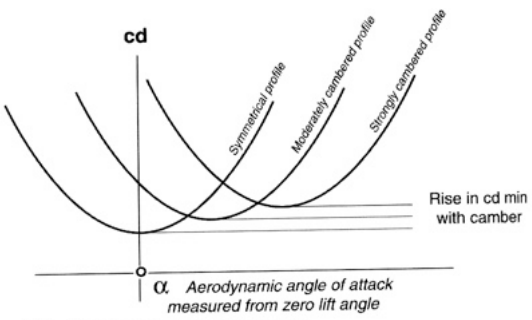

(A) Profile drag plotted against angle of attack

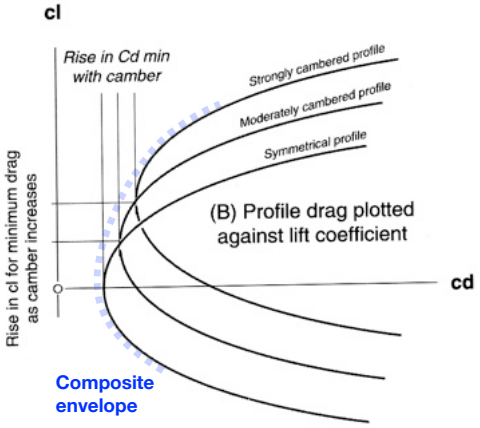

Effect on C_d of increasing camber:
1. $\alpha(C_{dmin})$ increases;
2. C_{dmin} increases;
3. **Drag polar moves up and right**.
   (note possibility of composite polar with variable geometry/flap: can exploit this to approximate the ideal polar across a range of design C_l.)

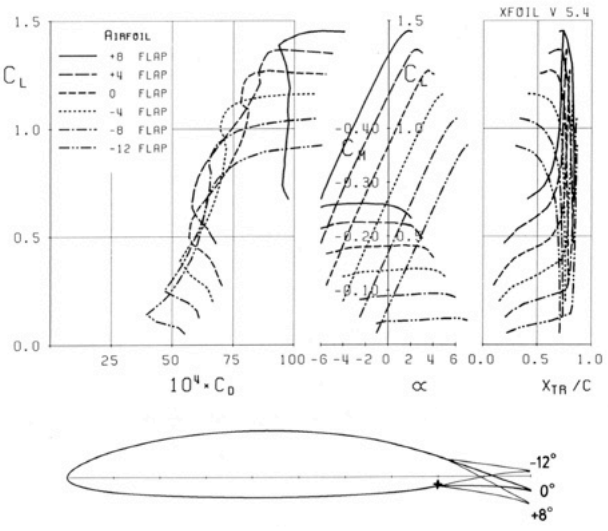

Fig. 1 Polars for laminar sailplane airfoil over range of flap settings [$Re = 10^6/\sqrt{(C_L)}$].

Influence of airfoil shape: camber distribution— 3

The effect of camber distribution (vs. amount of camber):

Generally, the airfoil 'works hardest' i.e. has the greatest difference between suction and pressure C_p where the curvature of the camber distribution is greatest. This also affects C_{lmax}: generally, higher C_{lmax} is achieved when the maximum camber is closer to the LE.

This characteristic is exploited in the design of 'supercritical' airfoils, where there is little camber near the LE to reduce recompression shock strength (and transition/separation), but camber is increased near TE to provide adequate overall C_l.

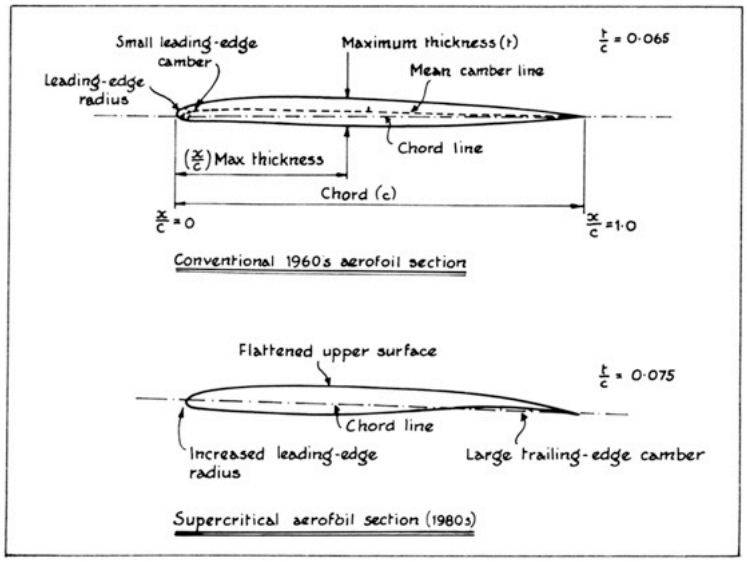

Influence of airfoil shape: thickness distribution — 1

Generalizations:

Camber distribution is typically chosen to generate minimum drag at a desired C_l, and/or C_{lmax}.
Thickness distribution is typically chosen to influence boundary layer and shock-wave behaviour.

1. The thickness distribution has 3 main determinants:
   (i) maximum thickness ratio;
   (ii) LE radius;
   (iii) chordwise position of maximum thickness.

2. The effect of these factors also depends on Reynolds and Mach numbers, making further generalization difficult. To simplify matters, break up consideration based on Mach number.

Subsonic/incompressible flow

1. Even quite thick airfoil sections can have rather low drag.

Same profile drag @ Re=6×10⁶

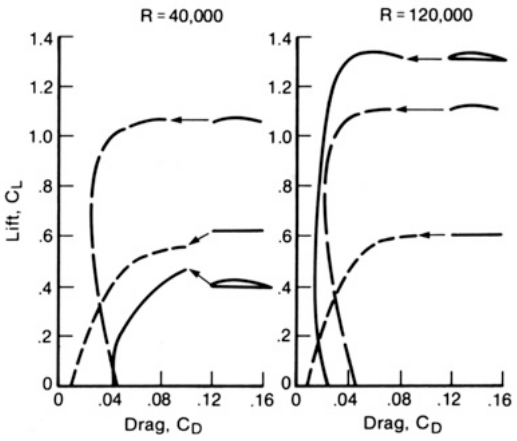

Wire

2. Historically, very thin airfoils were used first, largely because they had better performance at the comparatively low Reynolds numbers which could be achieved in early wind tunnel and other tests (e.g. by the Wright Brothers). Recognition that much thicker airfoils were aerodynamically (as well as structurally) preferable was a key advance in airfoil selection at around the time of WW1.

Above all but lowest Re, moderately thick airfoils have both higher C_{lmax} **and** higher $(L/D)_{max}$ than very thin ones.

Influence of airfoil shape: thickness distribution — 2

5. By changing the chordwise distribution of thickness we can affect the zero-α pressure distribution and hence the proportion of chord over which a favourable pressure gradient (and laminar flow, low drag) can be maintained.

This is the basis of laminar-flow airfoil design, which began with the NACA 6-series airfoils and was the key advance in subsonic section design at around the time of WW2. The maximum thickness typically occurs at approximately mid-chord, and the favourable pressure gradient is maintained somewhat further aft than this. In good conditions, transition will (hopefully) occur around this point.

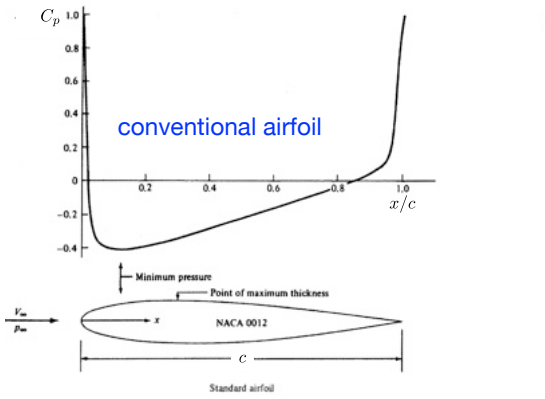

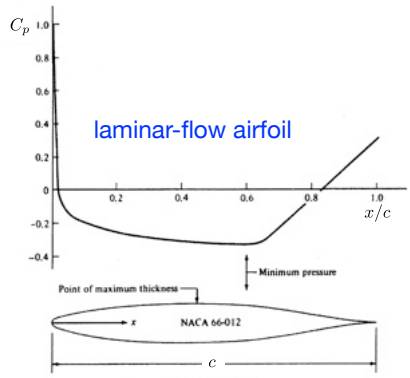

Measurements of skin friction for a laminar flow airfoil, NACA 27-212

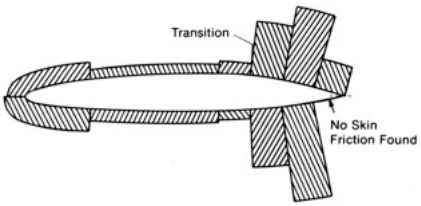

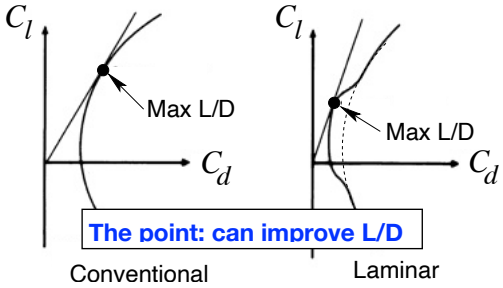

Influence of airfoil shape: thickness distribution — 2

3. While moderate thickness is an advantage, further increases ultimately must produce increasingly adverse pressure gradients, and bring about flow separation. There is a 'happy medium' range of *t/c* for subsonic (a.k.a. low speed) airfoils, typically of order 8-16%: optimal *t/c* gives best $C_{l\max}$.

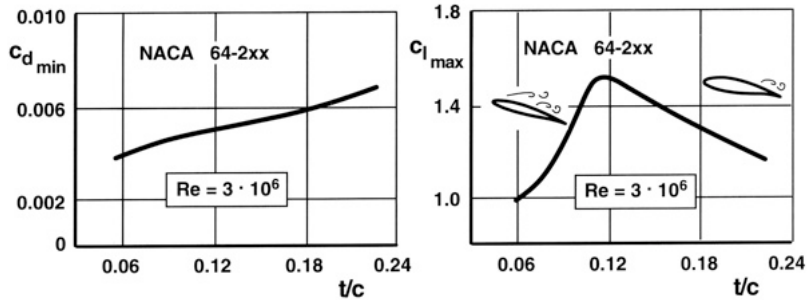

Lower t/c gives smaller minimum drag but also sharply reduces $C_{l\max}$ and gives poor/sharp (LE) stall characteristics.

4. Likewise there is an optimal leading edge radius for $C_{l\max}$. One measure is the relative thickness at 0.05*c*, i.e. the thickness at 5% chord as a proportion of maximum thickness, called z_5/t. (Must be < 1!).

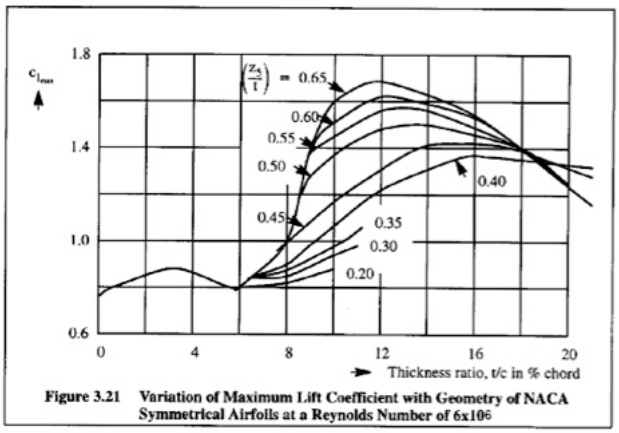

Figure 3.21 Variation of Maximum Lift Coefficient with Geometry of NACA Symmetrical Airfoils at a Reynolds Number of 6x10⁶

Good values of z_5/c are moderately high, of order 0.5.

NB: This feature is very *Re*-dependent. Optimal nose radius tends to reduce as *Re* falls.

Influence of airfoil shape: thickness distribution — 3

6. In practice, very good control of surface quality/roughness is required for laminar flow to be maintained to the design transition point (even small surface waviness can promote T-S wave instabilities). However, with modern moulded manufacturing this may be achievable with care.

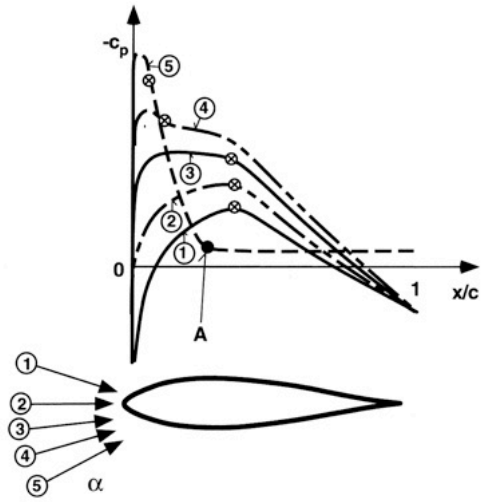

Fig. 43: Pressure distribution over a symmetrical airfoil at various angles of attack.

① - ⑤ upper surface pressure distribution at various angles of attack (see also Fig. 44)
② zero angle of attack, upper and lower surface pressure distribution
⊗ boundary-layer transition point
A separation point

7. Laminar flow can only be maintained around a range of α for a given camber and thickness distribution, because the pressure distribution changes with α.

Influence of airfoil shape: thickness distribution — 4

8. The design range of α or C_l over which laminar flow can be maintained for a given airfoil is known as the laminar bucket or drag bucket.

Effect of camber

Symmetric Cambered

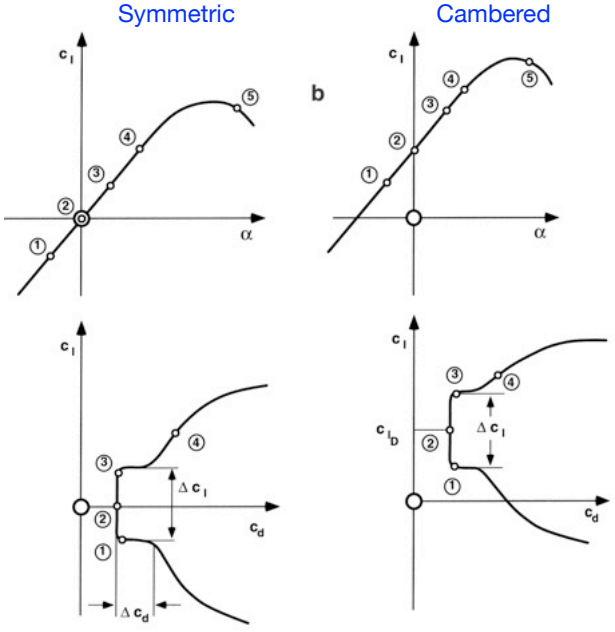

Camber shifts bucket to design lift coefficient.

Effect of thickness

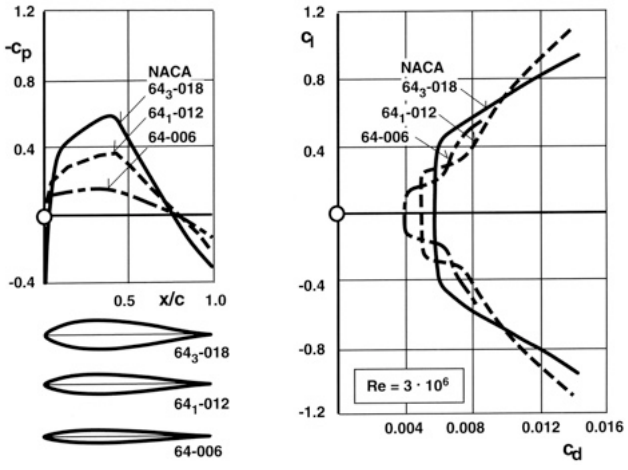

Thicker airfoils have a wider usable range of C_l but obtain less benefit from laminar flow.

Influence of airfoil shape: thickness distribution — 5

Transonic flow

1. Design to avoid/minimize shocks: profile and wave drag

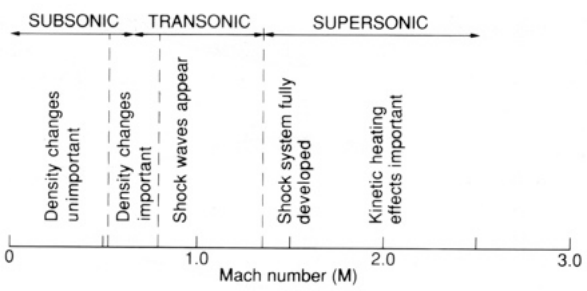

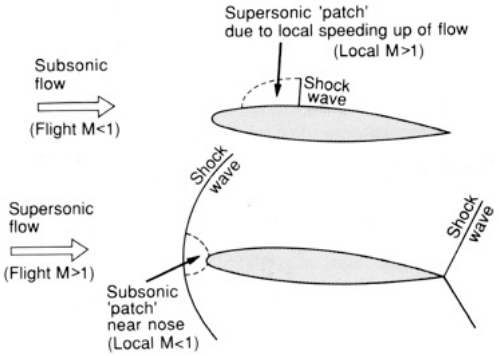

2. Both lift and drag increase in the transonic range. **So maximum $M_\infty L/D$ occurs in this regime.**

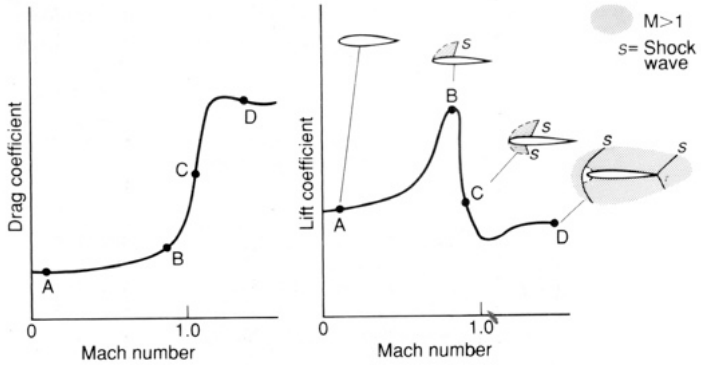

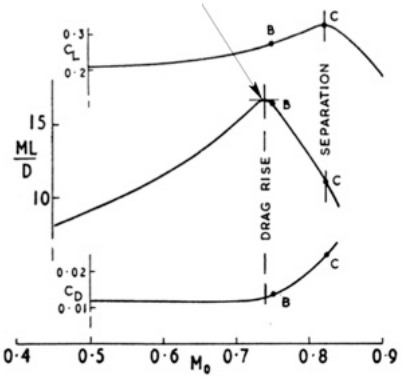

Influence of airfoil shape: thickness distribution — 6

3. Reducing thickness increases critical Mach number, where M=1 locally.

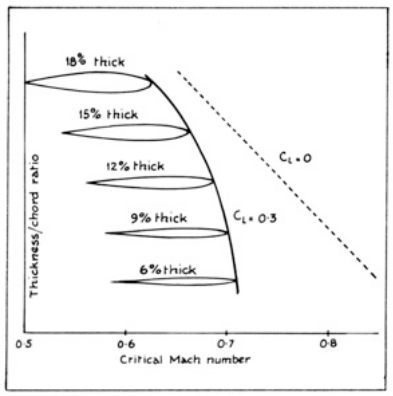

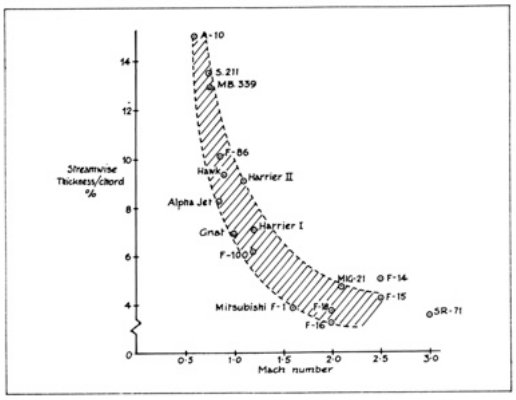

4. Supercritical airfoils are designed to have weak recompression shocks and increase the critical M_∞.

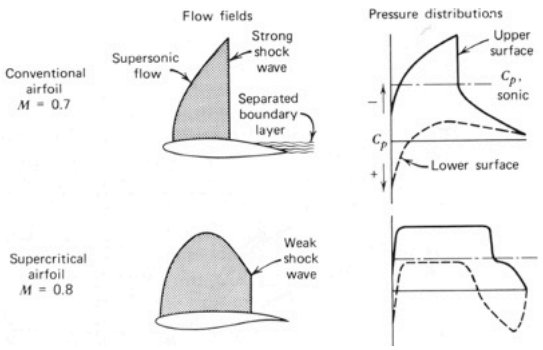

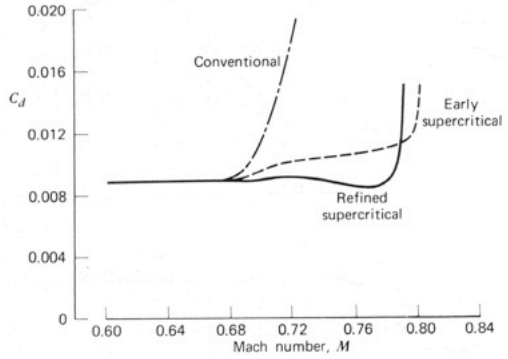

Influence of airfoil shape: thickness distribution — 7

Supersonic flow

Zero-lift pressure distribution

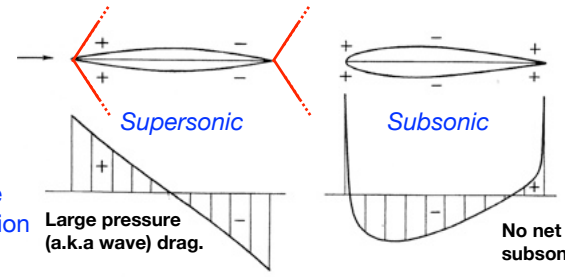

Large pressure (a.k.a wave) drag.

No net pressure drag in subsonic frictionless flow.

Lifting flow

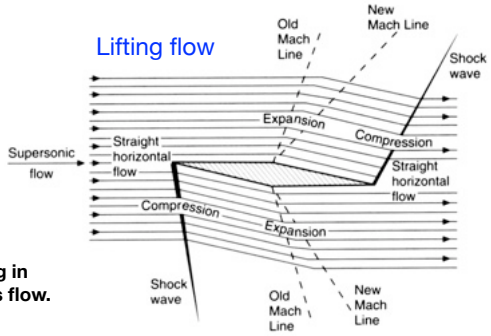

1. Design to minimize wave drag, proportional to α^2 and $(t/c)^2$ — supersonic airfoils are very thin.

2. Shocks and expansions can produce abrupt changes in flow direction so that flow separation is paradoxically a less important consideration at supersonic speeds than at subsonic — however supersonic airfoils can perform very poorly at subsonic speeds.

3. Lift production mechanism is different than for subsonic flow and **both** the centre of pressure and the aerodynamic centre lie at approximately $c/2$.

Lifting flow pressure distributions

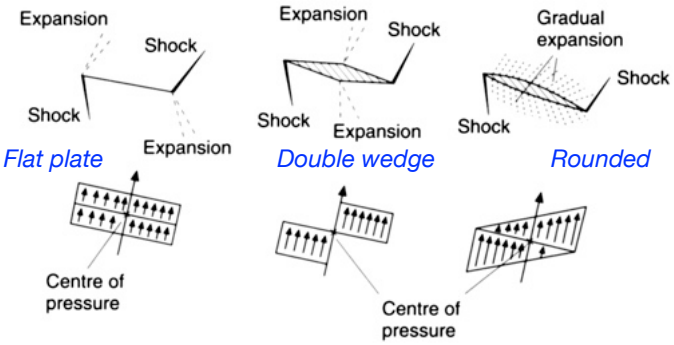

The movement of centre of pressure (typically rearwards) in supersonic flow can have important consequences for trim changes and trim drag.